Georgia Institute of Technology

AE8900 Special Problems

Trajectory Trade-space Design for Robotic Entry at Titan

Evan Roelke

Advised by

Dr. Robert Braun

Abstract

In recent years, scientific focus has emphasized other ocean worlds such as Europa, Enceladus, and Titan, due to their potential for harboring life. The only spacecraft ever to land on these moons was the Huygens Probe in 2005; however, this probe's main purpose was to study the atmosphere and surface of Titan, with no real landing target. Future missions to other ocean worlds would likely require a science target and thus add several constraints to the mission such as arrival time, entry state, and aeroshell geometry, among others. Of the three ocean worlds previously mentioned, Titan is an optimal target for initial mission concepts for several reasons. The atmospheric composition, winds, and surface features are well studied by Cassini and the Huygens Probe. Additionally, of the aforementioned moons, Titan does not have a thick ice sheet to penetrate in order to sample the surface and/or liquid seas, enabling such mission to double as a stepping stone for missions to other ocean worlds. Finally, Titan exhibits a myriad of interesting planetary features that, if studied, could further the understanding of both Titan's and the solar system's geologic history. In this paper we analyze the trade-spaces of various important parameters involved in Entry, Descent, and Landing (EDL) as it pertains to robotic missions for Titan in order to provide a guideline for optimizing a mission's system parameters while minimizing both system complexity and the landing footprint. It is found that the ideal geometry is a ballistic spherecone body entering from orbit to allow flexibility in the entry state vector. The aerothermodynamic environment is most affected by the entry velocity and the vehicle bluntness ratio, while the peak deceleration is most influenced by the entry velocity and entry flight path angle. In addition, multiple parachutes decrease the landing footprint, impact speed, and descent time compared to single parachute systems, at the expense of being more complex. Larger ballistic coefficients decrease the landing footprint and descent time while increasing the impact speed. Finally, it is discovered that the uncertainty in the entry altitude and flight path angle have the most impact on the final state vector.

Contents

1 Introduction

As scientific focus has shifted towards other ocean worlds in the solar system, new mission concepts to such bodies as Europa, Titan, or Enceladus will begin to pique global interest due to their potential for harboring life [2]. Few missions to these bodies have come to fruition, with the exception of the Huygens Probe in 2005, but the mission goal of Huygens was to study the atmosphere, winds, and surface features of Titan [7]. Therefore, any future missions to these moons that require precise targeting will need to be developed from scratch.

1.1 Titan Characteristics

Titan is Saturn's largest moon with a diameter of 5150km and a surface pressure of 1.5 bar [9]. It's surface temperature is 94 K and its surface gravity is a mere 1.35 m/s^2, resulting in an atmospheric scale height of 40km, compared to approximately 10km on Earth [6] [9]. The atmospheric interface altitude is estimated to be 1270km, which, combined with the low surface gravity and high surface pressure, categorically culminates into long descent times and large landing footprints [7]. Fortunately, the Cassini mission was able to map most of the moon's surface with radar, yielding several theoretically intriguing scientific targets [4]. A map of the northern hemisphere of Titan is shown in Figure 1. Among these includes the hydrocarbon seas, located mainly in the northern hemisphere, as shown in Figure 1.

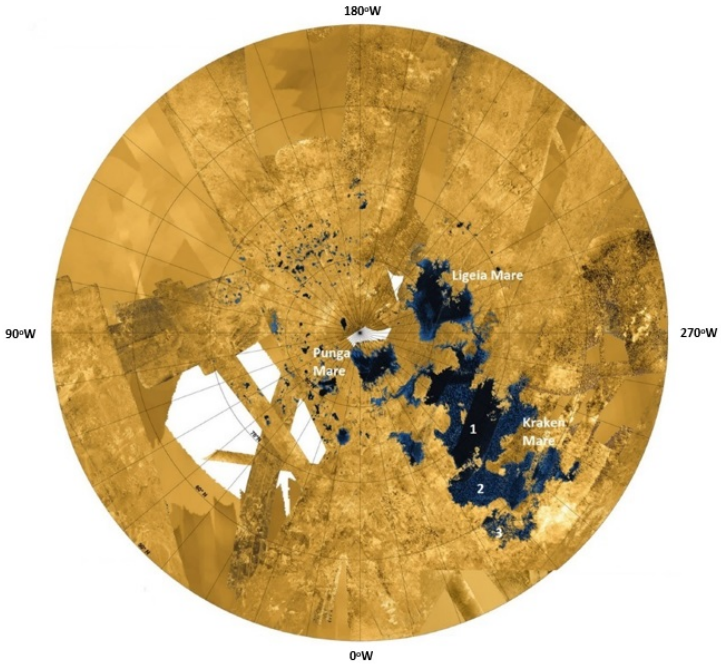

Figure 1: Cassini Radar Map of Titan's Northern Polar Region [4]

The investigations into TiME yielded conservative estimates for landing ellipses targeting the hydrocarbon seas for a range of possible arrival dates. Most of these dates and the associated acceptable footprints are limited to Titan springtime, occurring next in the early 2020s and then the late 2030s. Tidal forces from Saturn may cause these footprints to change significantly.

Ligeia Mare, the northern most sea centered at 78°, 245°W, allows for a dispersion of around 300 km × 120 km with 99% confidence, whereas Ontario Lacus, the largest sea in the southern hemisphere centered at 72°S, 178°W, yields a safe landing ellipse of approximately 80km × 60km. The largest sea on Titan, Kraken Mare, can be split into two bodies. The larger of which, distinguished as Kraken-1, is centered at 70.7°N, 308°W, yields the largest possible downrange error, with an acceptable footprint of 450km × 90km, although an ellipse of 240km × 200km has also been shown to be plausible, albeit less conservative depending on the ellipse orientation. The smaller sea, Kraken-2, which is located at 65°N, 324°W, has an acceptable ellipse of 270km × 100km. Finally, Punga Mare, the smallest of the major northern seas located at 85°N, 340°W, yields a safe landing ellipse of 120km × 120km, with a maximum possible error of 190km × 70km with ideal ellipse orientation [10]. All of these seas are potential landing targets and should be considered as such in Section 3.

It should be noted that the downrange and crossrange error ellipse orientation is dependent on the entry azimuth and entry flight path angle and as such, the aforementioned acceptable error ellipses are rough estimates. This puts an added constraint on the mission design, because if an entry vehicle enters the atmosphere directly from the interplanetary trajectory, the entry state vector is largely constrained by launch and arrival dates, which may also be important mission parameters if surface light is desired. However, if the aeroshell enters from orbit there is much more control over the entry state vector, including latitude, longitude, azimuth, and flight path angle. All of the simulations performed in this investigation use the same azimuth as the Huygens Probe, which was 88.89° [7].

1.2 Mission History

The argument for sending future probes to Titan is bolstered by the success of the Huygens Probe, while the unique moon also exhibits interesting geological features that could lead to a deeper understanding of the geologic history of our solar system [5]. Missions to this moon could also be utilized as a stepping stone, of sorts, to other ocean worlds. Firstly, Titan is not covered in a thick ice sheet like Europa or Enceladus, meaning that it is much easier to access the

liquid seas and oceans. In addition, Huygens and Cassini have provided valuable information about the atmosphere, winds, and surface features such as tides, ocean surface speeds, potential glaciers, and hydrocarbon mole fractions. Even though Titan does not have liquid water, which is generally thought to be the first indication of life, there is speculation that the hydrocarbon seas could harbor evidence of prebiotic chemistry [16]. Finally, developing technology that can operate in methane-diffused, liquid hydrocarbon seas inherently drives scientific discovery into the dynamics and chemistry of such liquid bodies that can be applied to our understanding of Titan and other planets with similar atmospheric/hydrologic features. Similarly, understanding Titan's geologic history could bolster knowledge about both its own formation and that of the solar system.

While the Huygens probe has been the only mission that has flown to Titan, there have been several mission concepts in the past decade, such as the Titan Mare Explorer (TiME), a NASA Innovative Advanced Concept (NIAC) study considering a Titan Submarine, and both a lake probe and hot air balloon as part of the ESA/NASA Titan Saturn System Mission (TSSM) [16] [4] [14]. TiME would attempt to land a capsule on Ligeia Mare (80°N), the second largest hydrocarbon sea in the northern hemisphere of Titan to further understand the moon's methane cycle [16]. The NIAC study proposed landing a submarine in Kraken Mare (72°N) to explore the depths of the hydrocarbon seas. It postulated that the submarine could feasibly explore both Ligeia and Kraken Mare by allowing the ballast system to accommodate the different methane-ethane ratios [4]. Finally, the ESA TSSM mission proposes a lake probe, similar to TiME, to splashdown in Kraken Mare, in addition to a hot air balloon floating approximately 10km about the surface at a latitude of 20°N. These systems would attempt to understand Titan's methane cycle and detect any signs of prebiotic molecules [14].

1.3 Entry Vehicle Considerations

While robotic entry at Titan has been successful before, it remains a difficult problem. Titan's atmospheric density at the surface is roughly 5 times that of Earth, and its gravity is approximately 14% of Earth, yielding descent times on the order of a few hours [4]. While this worked well with the Huygens Probe's goal of obtaining atmospheric measurements, it can be problematic for precision targeting, as an entry vehicle could be blown several kilometers off-target by uncharacteristic winds or density gradients. The thick atmosphere also somewhat limits retrorocket capabilities, thus requiring the use of parachutes until more advanced decel-

erator technology is developed and tested. Additionally, the thick atmosphere necessitates a steep entry flight path angle, especially for low ballistic coefficient missions, a category that robotics tend to fall under. The ballistic coefficient is a ratio of inertial to aerodynamic forces and is defined in Equation 1 as

$$\beta = \frac{m}{C_D A_{ref}} \tag{1}$$

where m is the mass, C_D is the drag coefficient, and A_{ref} is the projected reference area, which is typically calculated using the base radius. The steep flight path angle increases the stagnation point heat rate and peak deceleration, while the long descent times increase the total trajectory-integrated heat load. Larger peak heat rates typically decrease the total heat load because larger heat rates are typically an indication of a larger ballistic coefficient or steeper entry flight path angle, causing the descent time through the heating environment to become shortened. The large peak heat rate and heat load inevitably will constrain the thermal protection system (TPS) material, as well as the TPS thickness, reducing total mass allotted to the payload. Too large of a peak deceleration could cause the vehicle's structural mass ratio to increase and potentially damage the payload. In general, larger ballistic coefficients and steeper payloads increase the peak deceleration which occurs lower in the atmosphere.

Additionally, one must consider the entry vehicle geometry and aerodynamics. The Huygens Probe was a ballistic entry vehicle, meaning that the aeroshell flew at an angle of attack of 0° and thus produced no lift force. These systems are the simplest in the sense that the vehicle is limited in its guidance options in the hypersonic regime. In addition, it does not require any ballast mass to offset the vehicle center of mass in order to fly at an angle relative to the flow field.

However, entry systems that fly at an angle of attack to produce a lift force can be beneficial for guidance and control purposes. One such method is called bank angle control; by rotating the lift vector about the velocity vector, one can steer the entry vehicle out of plane. This is accompanied by a loss of vertical lift force, causing the entry vehicle to drop through the atmosphere at a higher rate, effectively limiting the vehicle's crossrange capability. This method can also be used to control the vehicle's downrange coverage through a series of "S-turns."

Unfortunately, such entry systems are typically more complex than ballistic entry vehicles, increasing the chances of a mechanism failure during entry. Second, the angle of attack must be

shallow enough in order to keep the flow stagnation point attached to the vehicle nose, or else the aeroshell may face heating and stability issues. In addition, in order for typical spherecones to fly at an angle of attack, additional ballast mass must be appropriated to keep the center of mass along the launch vehicle nose during takeoff, ejected from the entry vehicle before atmospheric entry, and then again added to the vehicle during the parachute descent stage of EDL to keep the center of mass along the vehicle nose. This is a lot of undesirable wasted mass that may further constrain the scientific payload and other mission parameters.

While offsetting the center of mass can be advantageous in order to bank the vehicle's lift vector about the velocity for guidance and control, such systems would not be as useful on a planetary body such as Titan due to its thick atmosphere and large scale height. Bank angle modulation has traditionally been performed during hypersonic flight until a supersonic decelerator is required for stability. Unfortunately, the supersonic flight regime on Titan occurs over a hundred kilometers from the surface, allowing unpredictable winds to guide the vehicle off course once again. Significant statistical confidence in Titan wind speeds is likely necessary before bank angle modulation should be considered a viable option.

In the end, there are inherent trade-offs between impact velocity, landing footprint, and parachute diameter, in addition to other parameters that may play an important role in the exploration of Titan. While a smaller nominal impact velocity is desirable to prevent damage to the payload, this will generally require a larger parachute diameter, thereby increasing the landing footprint. Because each mission concept will have varying constraints imposed upon the system, it would be useful to understand the relationships between parameters for any given entry system, especially when targeting constraints are added to the mission, as was the TiME, the NIAC submarine, and the TSSM lake probe. By understanding the relationships between the aeroshell geometry and aerodynamics, the entry velocity and flight path angle, the vehicle's ballistic coefficient, the uncertainty in the entry state vector, and the parachute systems including number of parachutes, parachute drag coefficient(s), parachute diameter(s), and parachute deployment triggers, one can more readily formulate a system to fit a mission concept requirement.

2 Methods

2.1 Computational Methods

Vehicle trajectories are computed using a Matlab solver developed by the Space Systems Design Laboratory at Georgia Tech. The solver uses a fourth order Range-Kutta method to integrate the equations of motion, which are defined in Equations 2a-2c below.

$$\frac{dV}{dt} = \frac{-\rho V^2}{2\beta} - g\sin\gamma \tag{2a}$$

$$V\frac{d\gamma}{dt} = \frac{V^2\cos\gamma}{r} + \frac{\rho V^2}{2\beta}\frac{L}{D} - g\cos\gamma \tag{2b}$$

$$\frac{dh}{dt} = \frac{dr}{dt} = V\sin\gamma \tag{2c}$$

where V is the velocity, t is time, ρ is the atmospheric density, β is the ballistic coefficient defined in Equation 1, g is gravity, γ is the flight path angle as measured from the local horizon, and $r = r_p + h$ is the entry vehicle position given a planet radius, r_p and an altitude, h.

Additionally, the stagnation point heat rate can be computed using Equation 3 below.

$$\dot{q_s} = k\sqrt{\frac{\rho}{r_n}}V^3 \tag{3}$$

where $\dot{q_s}$ is the stagnation point heat rate, k is the Sutton-Graves constant, and r_n is the vehicle nose radius [17].

Equations 2 and 3 are used extensively in this investigation to develop an understanding of the EDL tradespace for Titan. For each significant parameter of the tradespace that is varied, a Monte Carlo analysis is performed to assess the effect on the nominal trajectory parameters, the downrange and crossrange footprints, the maximum stagnation point heat rate, the maximum descent time, and the impact velocity and relevant statistical parameters. Insofar as parachute systems are concerned, only system with one and two parachutes are considered; a larger number of parachutes increases the complexity of the system and thus potential for system failure. In addition, multiple parachutes may or may not be necessary for a given mission concept and targeting requirement.

2.2 Wind Profiles

Tables of atmospheric data with altitude have been developed in TitanGRAM 2004 [6]. These tables are linearly interpolated to describe the pressure, density, temperature, and wind speeds as functions of altitude. While these tables are accurate for pressures, densities and temperatures, the wind profiles, as shown by Lorenz et. al., are nonphysical. The winds provided by these atmospheric tables produce an effect of infinite shear at the poles, resulting in a significant over-prediction of wind speeds [11] [10].

While a more realistic wind profile might contain some inherent sinusoidal behavior, this has not been observed or proven in the case of Titan. The more conservative approach of non-sinusoidal wind profiles is chosen as a result. The maximum, minimum, and nominal profiles are displayed in Figures 2a-2c below.

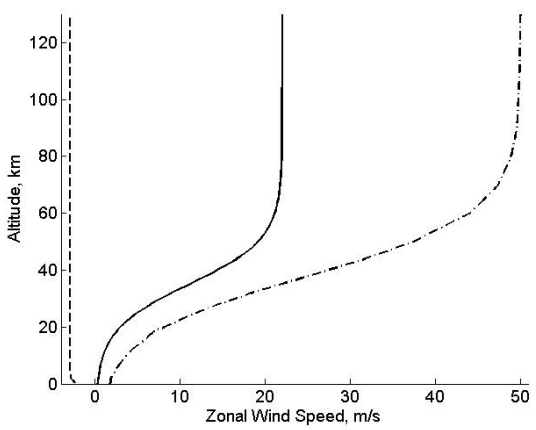

(a) Zonal Wind Profile Bounds

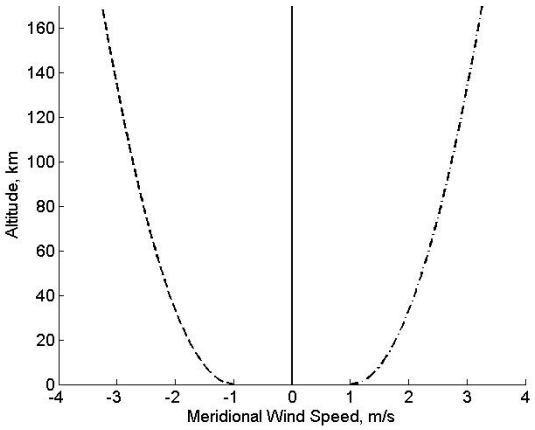

(b) Meridional Wind Profile Bounds

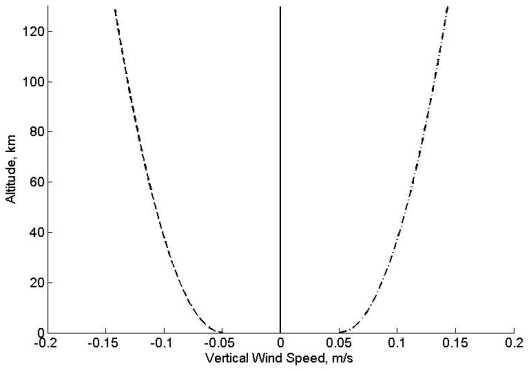

(c) Vertical Wind Profile Bounds

Figure 2: Wind Profile Bounds on Titan

The functions used to generate these wind profiles are taken directly from Lorenz et. al [11]. The nominal zonal winds can be described by Equation 4 below.

$$U(z) = \frac{U_{300}}{1 + \frac{1}{L}e^{z_0 - z}} \tag{4}$$

where U_{300} is the zonal wind speed at $300km$, z is the altitude in km, z_0 is the reference altitude, and L is the characteristic length scale. Nominal, maximum, and minimum bounds for each parameter are tabulated in reference [11], which are linearly interpolated with the TitanGRAM 2004 tables at each altitude point.

Subsequently, the nominal profiles are constrained between the tabulated minima and maxima bounds shown in Figure 2, and scaled by some arbitrary factor $|\alpha| < 1$ to represent an uncertainty profile. One thousand of these arbitrarily scaled wind profiles are generated and tabulated within TitanGRAM 2004 to be integrated into the Matlab simulations.

Similarly, the meridional wind bounds can be calculated with altitude using Equation 5 below, with z in km.

$$|V| = 1 + 3\sqrt{\frac{z}{300}} \tag{5}$$

The vertical wind profiles follow a similar pattern as the meridional winds with a nominal value of $0m/s$ with a standard deviation of $0.1m/s$. The profile of the vertical winds is assumed to be similar to that of the meridional winds to better capture the realistic evolution of vertical winds with altitude. The same procedure of generating one thousand differently scaled profiles is performed for the vertical and meridional winds.

It should be noted that the zonal wind profiles are the most significant of the vector elements, in addition to having the largest standard deviation, which will likely play a key role in influencing the entry vehicle's trajectory under $100km$ altitude.

2.3 Parameter Variations

As previously mentioned, the important independent variables under consideration are the entry state vector, the entry ballistic coefficient, the entry state vector uncertainty, the aeroshell geometry and associated aerodynamics, and the parachute system(s) including diameter(s), drag coefficient(s), and deployment triggers. The following sections will go into further detail about how each parameter is varied. For reference, the Huygens Probe was a $320kg$, $2.7m$ diameter, 60° sphere-cone with an associated ballistic coefficient of approximately $32kg/m^2$ [15]. It entered the Titan atmosphere at 1270 km above the surface at a velocity of $6km/s$ and a flight path angle

of $-65°$. The system consisted of three parachutes: a $2.59m$ Disk-Gap-Band (DGB) pilot chute, an $8.3m$ DGB main parachute, and a $3.03m$ stabilizing chute deployed at Mach 1.5, $100m/s$, and again at $100m/s$ once the vehicle underwent free fall without a parachute, respectively. Because more than two parachutes can be considered extraneous and increases system complexity, only single and double-parachute systems are considered in this investigation.

2.3.1 Entry State

The atmospheric interface at Titan is established to begin roughly at an altitude of $1270km$ [7]. Titan has a low escape velocity of approximately $2.6km/s$; therefore, entry velocities between 4 and $8km/s$ are considered to accommodate both direct entry and entry from orbit. Entry flight path angles at Titan generally must be steep in order to penetrate the thick atmosphere as much as possible before aerodynamic forces begin to dominate the trajectory. This is beneficial to decrease descent time, total integrated heat load, and potential for large landing footprints; however, it increases the maximum stagnation point heat rate, constraining the TPS thickness and material along with the entry state. Due to this, slight changes in the flight path angle could drastically alter the trajectory. To demonstrate this effect, the entry flight path angle is varied between $-50°$ and $-80°$. A flight path angle much shallower than this is not advised because it would drastically increase the descent time and landing footprint. In addition, a lifting body runs the possible risk of flying back out of the atmosphere at shallow angles of attack because of the low gravity and high atmospheric pressure.

The uncertainty of the entry state vector also plays a large role in the landing footprint and impact velocity, among other important mission factors. For reference, the 1σ entry uncertainties for the Huygens Probe were approximately 30 km, 3.37 m/s, and $0.28°$ in altitude, velocity, and flight path angle, respectively [7] [8]. These values correspond to 2.3%, 0.05%, and 0.43% of the respective entry state variables. In order to assess the investigated problem in a broad manner, the entry state 1σ uncertainties are varied within $\pm 1 - 2\%$ of the Huygens 1σ values.

2.3.2 Parachute Systems

As previously mentioned, systems comprised of one or two parachutes are considered in this investigation, even though the Huygens probe used three. This is because there is an inherent trade-off between the system complexity and desired mission parameters. For instance, staging multiple parachutes is ideal to perfectly control the trajectory of the probe in terms of impact

velocity, landing footprint, and descent time, among other factors; however, each additional parachute adds another subsystem that is prone to failure, resulting in the failure of the overall system. Section 3 will seek to show that a system with two parachutes, or even a single parachute depending on the mission constraints, is sufficient for an acceptable descent time, landing footprint, and impact velocity. In order to generalize the results of this investigation, a new parameter called the diameter ratio is introduced. The diameter ratio is introduced in Equation 6 below.

$$\eta_D = \frac{D_{parachute}}{D_{areoshell}} \tag{6}$$

where $D_{parachute}$ is the diameter of the parachute in question (either the initial parachute, referred to as the Pilot chute, or the Main Parachute), and $D_{aeroshell}$ is the diameter of the aeroshell used to calculate the vehicle's reference area. The Pilot chute is typically used for stability in the supersonic flow regime in which hypersonic geometries become unstable. Thus, in two parachute systems it will generally have a diameter similar to that of the aeroshell to provide stability, but not add significant drag area.

In order to simplify some of the analysis, it will be assumed that the supersonic parachutes are Disk-Gap-Band (DGB) parachutes with a drag coefficient of 0.55. While other parachute designs with better drag coefficients exist, DGB parachutes have significant flight credibility and are not overly complicated. In addition, a large parachute drag coefficient is not necessarily desirable on Titan, as descent times are already on the order of several hours. Figure 3 below depicts the parachute configuration discussed in this investigation [1]. In this Diagram, H_G and H_B are the gap and band heights, respectively, D_B and D_V are the band and vent diameters, respectively, and L_S is the suspension line length connecting to the entry vehicle's backshell.

Finally, when presenting results for two parachute systems, the diameter ratio will generally refer to the ratio between the main (second) parachute and the aeroshell diameter.

2.3.3 Entry Configurations

The entry geometry, and thus the aerodynamics, ballistic coefficient, and trajectory, are all dependent on the payload dimensions, but constrained by the faring size on the launch vehicle. Typically, robotic payloads are contained within sphere-cone aeroshells, a heritage technology from the Viking missions. A typical aeroshell configuration is depicted in Figure 4 for reference,

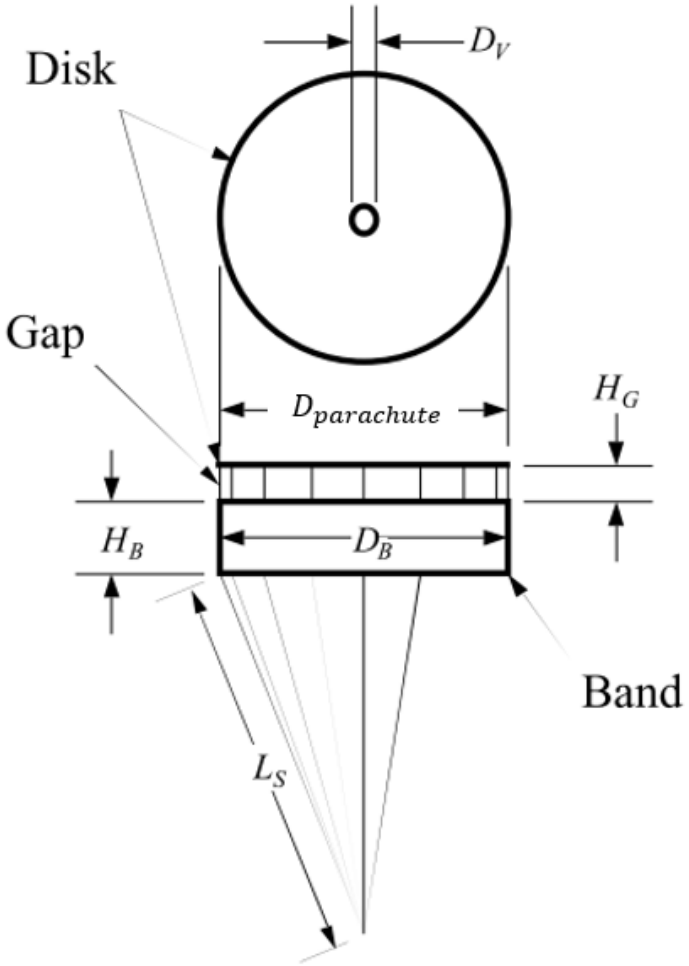

Figure 3: Disk-Gap-Band (DGB) Parachute Configuration [1]

depicting the angle of attack, α, half-cone angle, δ_C, the backshell radius, r_c, the nose radius, r_n, and the aeroshell diameter, $D_{aeroshell}$. These characteristics are the most readily altered on a typical spherecone, and thus Section 3 will investigate the effects of altering these parameters on various mission design constraints.

As missions to ocean worlds become more complex, they may begin to outgrow the traditional sphere-cone shape. The geometric design of the entry aeroshell can play an important role in not only the vehicle aerodynamics, but also the aerothermodynamic environment experienced by the spacecraft throughout the hypersonic flight regime. Examples of important factors include the nose radius, base radius, and half-cone angle for a traditional sphere-cone shape. In addition, the angle of attack will move the flow stagnation point around the vehicle nose. If the nose radius is too small and the angle of attack too high, the stagnation point will move off of the nose, which can severely detriment the aeroshell. In an atmospheric environment as dense as Titan's, slight changes in the geometry intended for aerodynamic benefits can have

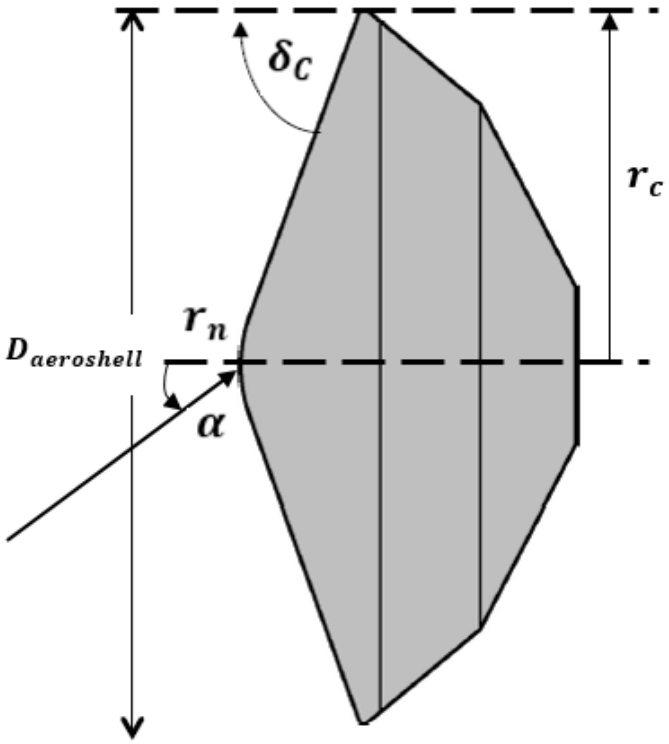

Figure 4: Spherecone Aeroshell Configuration

drastic effects on the aerothermodynamics of an entry vehicle. To better assess changes in the vehicle aerodynamics, the non-dimensional parameter bluntness ratio is introduced in Equation 7 below.

$$b = \frac{r_n}{r_c} \tag{7}$$

where r_n is the nose radius, and r_c is the base radius. The hypersonic aerodynamic coefficients for blunted sphere-cone bodies can be analytically calculated using the expressions in Equations 8a-8d below, which are a manifestation of Newtonian fluid dynamics.

$$C_L = C_N \cos\alpha - C_A \sin\alpha \tag{8a}$$

$$C_D = C_A \cos\alpha + C_N \sin\alpha \tag{8b}$$

$$C_N = [1 - b^2 \cos\delta_c] \cos^2\delta_c \sin 2\alpha \tag{8c}$$

$$C_A = b^2[1 - \sin^4\delta_c] + [2\sin^2\delta_c \cos^2\alpha + \cos^2\delta_c \sin^2\alpha][1 - b^2\cos^2\delta_c] \tag{8d}$$

where C_L and C_D are the lift and drag coefficients, respectively, C_N and C_A are the normal and axial coefficients, respectively, δ_c is the half-cone angle, and α is the angle of attack. It is clear from studying these equations that, in general, increasing the bluntness ratio of the vehicle will increase its drag coefficient and thus decrease its overall lift-to-drag ratio, $\frac{C_L}{C_D}$. In addition, the entry vehicle diameter is constrained by launch vehicle dimensions; the current maximum payload fairing diameter is 5 meters on the Atlas V [18]. For example, the NIAC submarine study initially investigated a slender, 6 meter-long shape, requiring the use of uniquely-shaped entry geometries [4]. These uniquely-shaped hypersonic vehicles would generally have very different aerodynamic coefficients and reference areas than sphere-cone shapes due to the nature of the payloads they are designed for. Examples of such vehicles include the Aero-Maneuvering Orbit to Orbit Shuttle (AMOOS) [12] [19], Saturn Orbiter Dual Probe (SO2P) [3], and the ESA IXV [13]. These vehicles are attributed with unique lift-to-drag ratios that might considerably alter the trajectory on Titan compared to a ballistic entry vehicle. These slender bodies generally also have a smaller back shell diameter and fly at a high angle of attack, potentially significantly changing the vehicle's ballistic coefficient.

In order to accommodate a plethora of vehicle configurations and payload designs, this investigation will seek to study a large range of the trade-space. Fortunately, the ballistic coefficient provides a useful metric with which to compare vehicle designs without studying each parameter specifically. The Huygens Probe had a ballistic coefficient of $28.75 kg/m^2$ and the Mars Science Laboratory had a ballistic coefficient of approximately $120 kg/m^2$ [15]. Thus, the lowest ballistic coefficient considered is $25 kg/m^2$, while the largest is $400 kg/m^2$ to represent a heavy robotic mission. Additionally, three different lift-to-drag ratios are considered to broaden the generalization of this investigation: a ballistic vehicle ($\frac{L}{D} = 0$), a mid-$\frac{L}{D}$ vehicle ($\frac{L}{D} = 0.24$) which is quite similar to the lift-to-drag ratio of MSL, and a high-$\frac{L}{D}$ vehicle ($\frac{L}{D} = 1.17$) modeled after the aforementioned SO2P vehicle. The first two lifting bodies are attainable with spherecone geometries shown in Figure 4, while the SO2P entry configuration is shown in Figure 5 below [3].

Figure 5 shows the nose and backshell radii, r_n and r_c, respectively, in addition to the nose angle, θ_C. The nose angle is the angle of the nose relative to the main vehicle axis and is used in various SO2P configurations to provide varying coefficients of lift [3].

In all cases, the lift-to-drag ratio is inherently related to the geometry of the aeroshell, such as the nose radius, base radius, and half-cone angle; therefore, the different lifting bodies

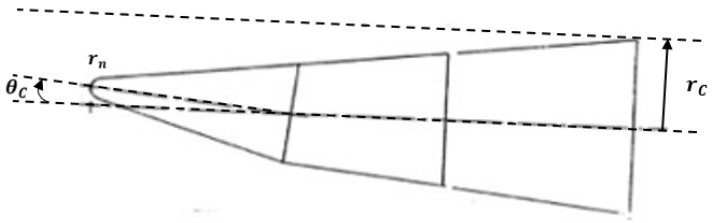

Figure 5: Saturn Dual Probe Orbiter Configuration [3]

previously described will fly through unique heating environments and descent trajectories, which may further constrain the entry state vector and mission parameters.

3 Results

3.1 Aerothermodynamics

The increased atmospheric density and pressure on Titan relative to Earth play a critical role in an entry vehicle's aerothermodynamic environment. As mentioned in Section 2.2.1, Titan's atmosphere presents a potentially limiting heating environment due to its large scale height and surface density. The vehicle geometry, specifically the bluntness ratio, will affect not only the aerodynamics, but also the atmospheric heating environment through which it must fly. The following results seek to analyze the maximum expected peak stagnation point heat rate, defined in Equation 3, as functions of various parameters that may influence its value, such as the vehicle bluntness, the entry ballistic coefficient, and the entry state vector. It should be noted that the total integrated heat load, which determines the thickness of the TPS, is generally lower for larger peak heat rates.

Figures 6a and 6b below display the relation between bluntness ratio and the maximum stagnation point heat rate and total integrated heat load for various entry velocities. Each simulation was ran using a Monte Carlo analysis and as such, each data point shows the maximum expected peak stagnation point heat rate with 95% confidence.

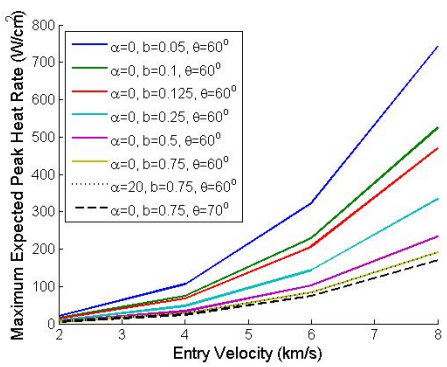

(a) Peak Heat Rate vs. Entry Velocity, $\beta = 200$

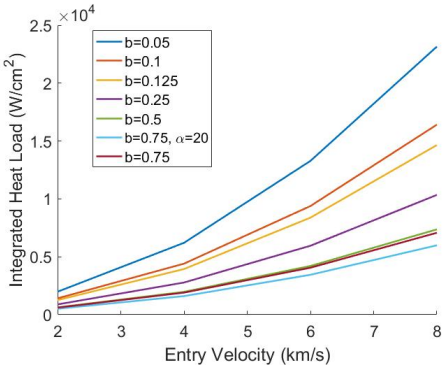

(b) Integrated Heat Load vs. Entry Velocity, $\beta = 200$

Figure 6: Heating Parameters vs. Entry Velocity for several Bluntness Ratios

The ballistic coefficients for each of these cases remained constant, demonstrating that decreasing the bluntness ratio causes a significant rise in the peak stagnation point heat rate, ultimately becoming a limiting factor for both high entry velocities and sharp-nosed vehicles. This is expected because as the nose becomes sharper, the shock becomes weaker, resulting in more energy being transferred to the vehicle surface rather than its wake. It should also

be noted that increasing the entry velocity causes an exponential-like increase in the peak stagnation point heat rate. This can potentially constrain the interplanetary trajectory of the mission depending on the expected entry ballistic coefficient and may require entry from orbit rather than direct entry.

Figure 6b shows the total integrated heat load against the entry velocity for various bluntness ratios. While a higher peak heat rate typically causes the integrated heat load to decrease, the same trends from Figure 6a can be seen here; larger entry velocities and sharper-nosed vehicles increase the total integrated heat load.

Furthermore, Figure 6a demonstrates that flying at an angle of attack with respect to the flow field has little effect on the maximum expected peak heat rate. Even though flying at an angle of attack will slightly alter the vehicle's aerodynamics and thus the ballistic coefficient according to Equations 8 and 1, the effect is minimal because angles of attack are shallow enough to have a small effect on $\sin\alpha$. However, significant changes in the half-cone angle, δ_c, have a noticeable effect, as shown by the dashed black line in Figure 6a, especially when raised to a power as in Equation 8. The wider half-cone angle will increase the overall coefficient of drag to a noticeable enough degree that the peak heat rate is slightly decreased. Of course, the increased drag coefficient may also propagate through the equations of motion to increase the total descent time and potentially the landing footprint.

In order to assess the effect of the ballistic coefficient on the vehicle aerothermodynamics environment, Figure 7 displays the peak stagnation point heat rate for several different ballistic coefficients as a function of entry velocity. It should be noted that in the following cases, the bluntness ratio remained constant to isolate the influence of the ballistic coefficient.

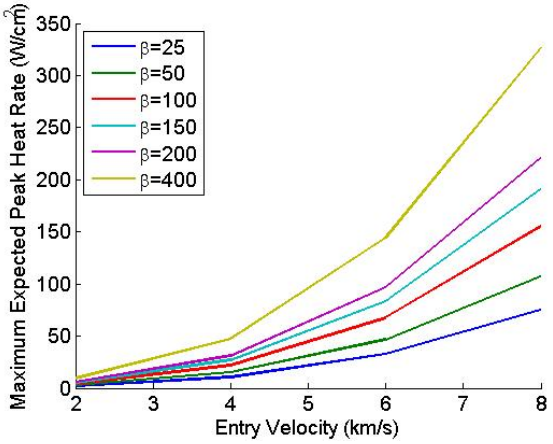

Figure 7: Peak Heat Rate vs. Entry Velocity for Various Ballistic Coefficients, $b = 0.5$

Figure 7 shows that a larger ballistic coefficient tends to increase the peak stagnation point heat rate, although not as severely as the bluntness ratio. In addition, it displays the same exponential increase in peak heat rate as the entry velocity is increased. Of course, a low ballistic coefficient isn't necessarily desired, because it typically means a reduced payload mass. In addition, a smaller ballistic coefficient will drive the mission's total descent time, and potentially landing footprint, up significantly; however, this will be discussed in more detail in Section 3.3. Clearly, the bluntness ratio has a much larger impact on the peak heat rate than the ballistic coefficient does; fortunately, the geometry of the aeroshell tends to be more flexible from a design standpoint than the entry ballistic coefficient.

As mentioned in Section 1.3, the entry flight path angle is expected to have a significant impact on the maximum expected peak stagnation point heat rate and be especially variant over a range of different ballistic coefficients. It is also expected to thus play an important role in the total integrated heat load. To demonstrate these effects, Figure 8 plots the maximum expected peak stagnation point heat rate and total integrated heat load as a function of the entry flight path angle for various ballistic coefficients.

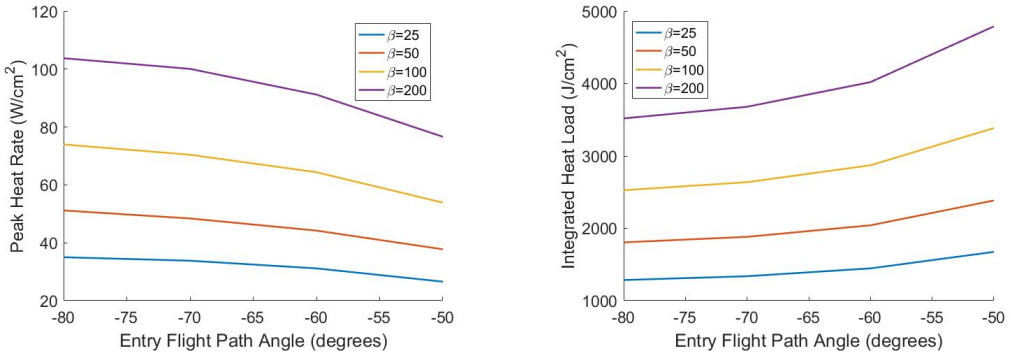

(a) Peak Heat Rate vs. Entry Flight Path Angle

(b) Integrated Heat Load vs. Entry Flight Path Angle

Figure 8: Heating Parameters vs. Entry Flight Path Angle for Various Ballistic Coefficients

Indeed, the entry flight path angle does play a noticeable role in the maximum expected peak heat rate. Shallower entry flight path angles decrease the maximum peak heat rate, while larger ballistic coefficients also increase the maximum peak heat rate, as expected. The relative decrease in the peak heat rate is likely non-mission constraining because the peak heat rate tends to increase by only 10-20 W/cm^2 over the range of analyzed entry flight path angles, even for a large ballistic coefficient such as $200\frac{kg}{m^2}$. While shallower entry flight path angles decrease the peak heat rate, they are more likely to increase the descent time and landing footprint as

analyzed in Section 3.3.

Additionally, Figure 8b shows that the total integrated heat load increases for shallower flight path angles. This is because, as mentioned in Section 1.3, a steeper entry flight path angle will decrease the total time that the vehicle is traveling at hypersonic speeds where the majority of the heating takes place. Therefore, while the entry flight path angle increases the peak heat rate, it decrease the total heat load and thus decreases the thickness of the TPS. It is also noted that larger ballistic coefficients increase both the peak heat rate and total integrated heat load, constraining both the TPS material and thickness.

Similarly, it is advantageous to understand how the inevitable uncertainty in the entry flight path angle propagates throughout the equations of motion and the influence on important mission parameters. Figure 9 shows the affect on the maximum expected peak stagnation point heat rate and heat load plotted against variations in the uncertainty in the entry flight path angle as a function of two different ballistic coefficients. As mentioned in Section 2.3.1, the 1σ uncertainty in the entry flight path angle for Huygens was 0.28^o, or 0.43% of the entry flight path angle [7].

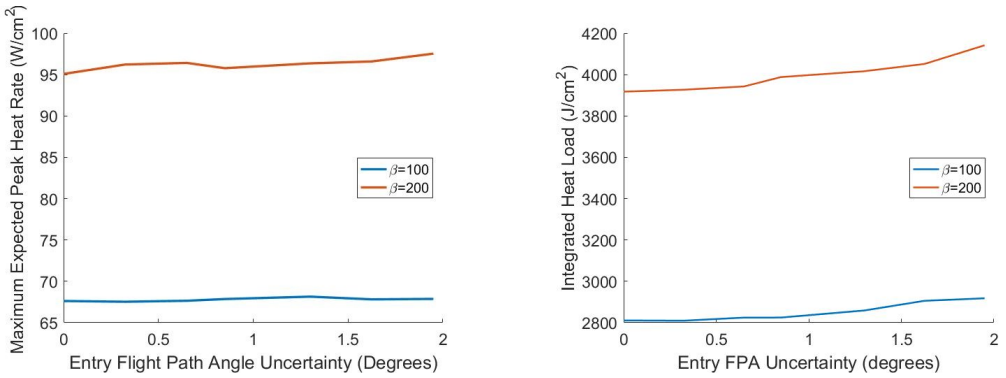

(a) Peak Heat Rate vs. Entry Flight Path Angle Uncertainty

(b) Integrated Heat Load vs. Entry Flight Path Angle Uncertainty

Figure 9: Heating Parameters vs. Entry Flight Path Angle Uncertainty for Various Ballistic Coefficients

Figure 9a demonstrates that the uncertainty in the entry flight path angle plays a largely negligible role in the maximum expected peak stagnation point heat rate. It is possible that for higher ballistic coefficient missions, the uncertainty in the entry flight path angle may have a significant effect on the peak heat rate given that the slope of the curve is steeper for an entry ballistic coefficient of $400\frac{kg}{m^2}$ than $200\frac{kg}{m^2}$; however, this would likely be the case for ballistic coefficients outside the realm of robotic missions.

In addition, Figure 9b shows that the uncertainty in the flight path angle plays a noticeable,

yet small role in the total integrated heat load. As analyzed from Figure 8b, the shallower flight path angles increase the total heat load. In this case, a larger uncertainty in the entry flight path angle causes an increase in the maximum expected total integrated heat load for both ballistic coefficients plotted.

Therefore, it is clear that the largest effect on the peak stagnation point heat rate and total integrated heat load is the entry velocity. The vehicle bluntness ratio is the second biggest factor in the peak stagnation point heat rate, while the entry flight path angle is the second biggest factor for the total integrated heat load. The entry velocity is likely to be much more constrained by the mission time-frame than the other parameters; although, fortunately the bluntness ratio is typically a flexible design parameter and should not significantly hinder any mission designs. Finally, the ballistic coefficient plays a large role in the both heating parameters; however, variations in the ballistic coefficient become much more prominent at higher entry velocities. Thus, the entry velocity is likely the biggest mission constraint in terms of the aerothermodynamics environment.

It is expected that the entry flight path angle uncertainty will have a much larger impact on the vehicle when propagated through the entire trajectory, which will be discussed in Sections 3.3.4 and 3.4.4; however, entry systems equipped with a single parachute will be analyzed first.

3.2 Deceleration

As discussed in Section 1.3, the vehicle's peak deceleration can constrain the entry vehicle by increasing the structural mass fraction, potentially decreasing the payload mass or other vehicle features. Too large of a deceleration can limit the payload, as it must be able to survive the deceleration through the atmosphere, as well. In general, large ballistic coefficients and steep flight path angles are known to cause the vehicle to decrease lower in the atmosphere with a larger peak deceleration magnitude. Figure 10 plots the peak deceleration magnitude against the entry velocity for various ballistic coefficients. It should be noted that the peak deceleration occurs well before parachute inflation; therefore, assessing the trends for each type of parachute system is redundant.

As shown in Figure 10, the ballistic coefficient does not play as large of a role in the peak deceleration as initially theorized. Instead, the entry velocity plays a much bigger role, with an exponential-like increase in the peak deceleration with increasing entry velocity, much like the trend seen in Figure 6 in Section 3.1. In order to assess the other claim that the entry flight

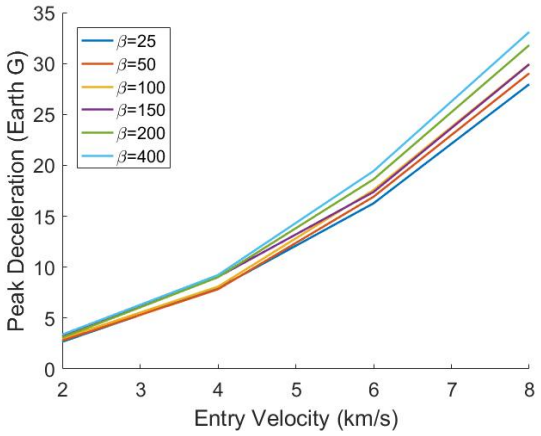

Figure 10: Peak Deceleration vs. Entry Velocity for Various Ballistic Coefficients

path angle can have an affect on the peak deceleration, Figure 11a plots the peak deceleration against the entry flight path angle and Figure 11b plots against the uncertainty in the entry flight path angle for several ballistic coefficients.

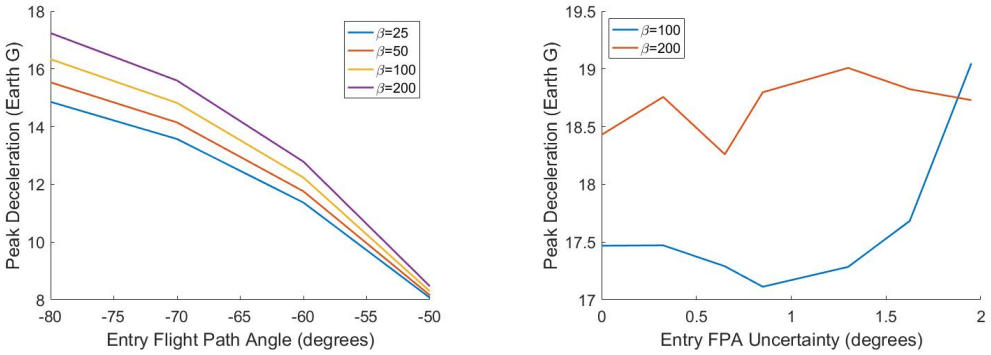

(a) Peak Deceleration vs. Entry Flight Path Angle

(b) Peak Deceleration vs. Entry Flight Path Angle Uncertainty

Figure 11: Peak Deceleration vs. Flight Path Angle for Various Ballistic Coefficients

Figure 11 demonstrates that shallower entry flight path angle do decrease the maximum expected peak deceleration. Additionally, the variation in ballistic coefficient becomes much more prominent at steeper angles of attack. Thus, depending on the structural integrity of the aeroshell and payload, the mission may be constrained in terms of entry flight path and angle and ballistic coefficient based on the peak deceleration alone. Additionally, Figure 11b shows that uncertainty in the entry flight path angle has a tendency to increase the peak deceleration but the data is somewhat variable, especially for larger ballistic coefficients. This indicates that the uncertainty in the flight path angle is much less of a concern with regard to the peak deceleration than the entry velocity, entry flight path angle, or ballistic coefficient are.

3.3 Single Parachute Systems

As mentioned in Section 2.3.2, this investigation will cover single parachute systems, assuming a DGB parachute with a drag coefficient of 0.55. Some missions might prefer a single parachute to multiple for simplistic, reliable designs. In addition, the landing error might not be a vital mission constraint, in which case drifting through the atmosphere with a single parachute would likely be preferred to staged parachutes of different diameters.

Important considerations with parachute systems mainly include the diameter ratio, defined in Equation 6, uncertainties in the entry state vector, and the entry ballistic coefficient. Alterations in these parameters can have drastic effects on the landing footprint, impact speed, and total descent time of one's mission. Variations in the diameter ratio will be considered first across a range of lift capabilities. Finally, as with all EDL systems, the entry ballistic coefficient plays a large driving factor in the vehicle's trajectory as well. Therefore, a Monte Carlo analysis is done for a variety of vehicle configurations, parachute diameter ratios, and entry ballistic coefficients to understand the full scope of the tradespace.

The following sections will investigate the effect of the diameter ratio on several parameters, including the downrange and crossrange errors, the impact speed, and the total descent time. Heating parameters will not be discussed because the heating environment during parachute descent is negligible compared to that during hypersonic flight. The parameters that remain constant throughout the results analysis and between each Figure are derived from the Huygens Probe mission to most accurately model a realistic mission scenario.

3.3.1 Ballistic Entry

To begin, the effect of diameter ratio on downrange and crossrange footprints is analyzed. The downrange and crossrange errors can be interpreted as forming an elliptic region where the vehicle is 95% likely to land, where the downrange and crossrange errors are the semi-major and semi-minor axes of the ellipse. Figures 12a-12b depict the Downrange and Crossrange errors for a low and high entry velocity, respectively, each for a variety of ballistic coefficients.

These factors play a crucial role in a mission design. For example, if the science target is the hydrocarbon seas on Titan, the entry vehicle is constrained to a finite landing ellipse to ensure the vehicle hits the sea rather than land. There is little variation between Figures 12a and 12b, indicating that the entry velocity plays a less crucial role in the landing footprint than previously detailed.

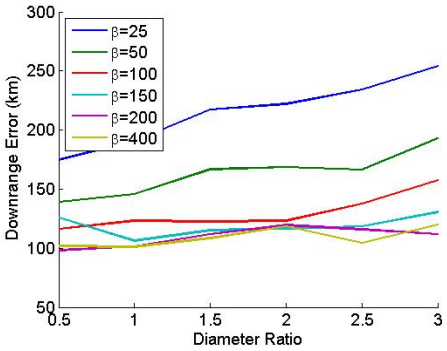

(a) Downrange Error for $V_{atm} = 4km/s$

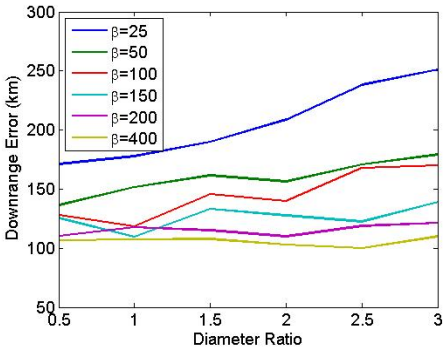

(b) Downrange Error for $V_{atm} = 8km/s$

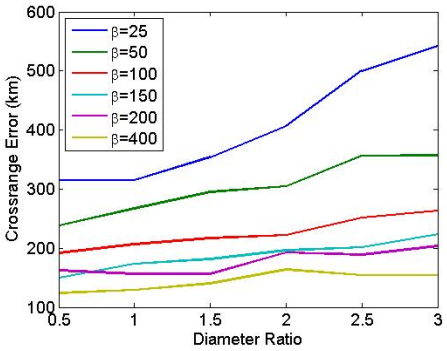

(c) Crossrange Error for $V_{atm} = 4km/s$

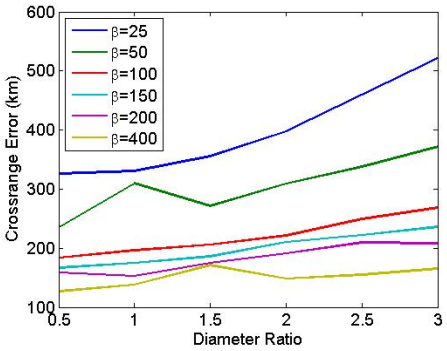

(d) Crossrange Error for $V_{atm} = 8km/s$

Figure 12: Downrange and Crossrange Error vs. Diameter Ratio for Single Parachute, Ballistic Entry Systems

The entry ballistic coefficient and diameter ratio also appear to play large roles in the landing footprint as well; however, it appears that the landing footprint between larger ballistic coefficients narrows considerably. In addition, the variation across diameter ratios tends to decrease for larger ballistic coefficients. Thus, if one were to require smaller landing footprints, some sort of guidance and control system would likely need to be implemented.

The effect of diameter ratio on the maximum expected impact speed and descent times is shown in Figures 13a-13d below. The data shown depicts the largest expected impact speeds with 95% confidence to accommodate conservative designs.

There are very distinct trends shown in Figure 13; specifically, larger diameter ratios decrease the maximum expected impact speed, but increase maximum expected descent times. Additionally, larger ballistic coefficients are responsible for increased impact speeds as well as decreased descent times. While there is an inherent trade-off between impact speed and descent time, the impact speed of the vehicle is much more of a design constraint than the descent time, as the vehicle must be able to withstand a certain magnitude of impact force, whereas an increased descent time typically does not constrain the mission. Of course, the increased

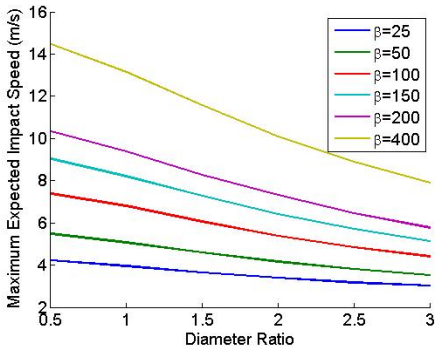

(a) Expected Impact Speed for $V_{atm} = 4km/s$

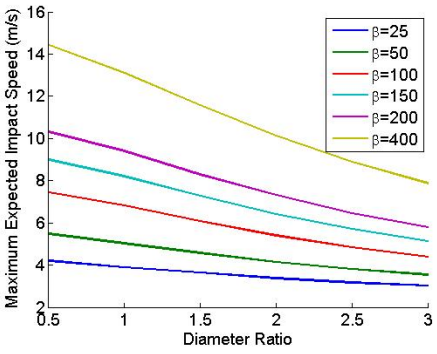

(b) Expected Impact Speed for $V_{atm} = 8km/s$

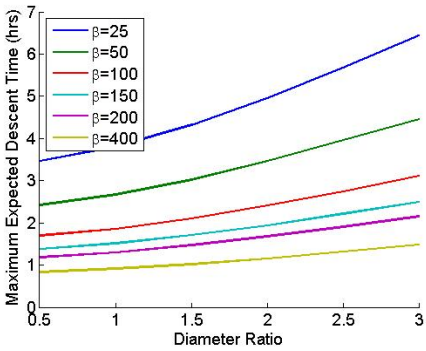

(c) Expected Descent Time for $V_{atm} = 4km/s$

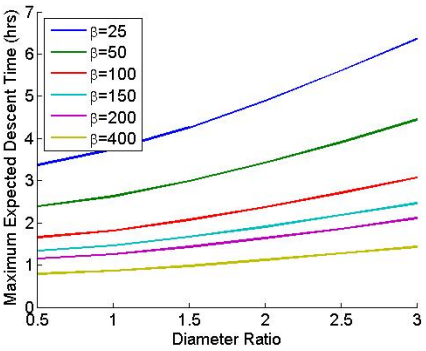

(d) Expected Descent Time for $V_{atm} = 8km/s$

Figure 13: Maximum Expected Impact Speed and Descent Time vs. Diameter Ratio for Single Parachute, Ballistic Entry Systems

landing footprint as a function of diameter ratio provides another trade-off between the landing error and impact speed; the severity of which is dependent on the specific mission requirements.

Finally, it is important to understand how the entry flight path angle affects the final state vector. The final state vector parameters under scrutiny are plotted against the entry flight path angle for a few ballistic coefficients in Figure 14.

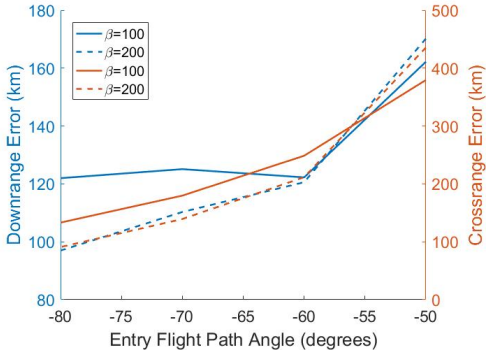

(a) Downrange and Crossrange Errors vs. Entry Flight Path Angle

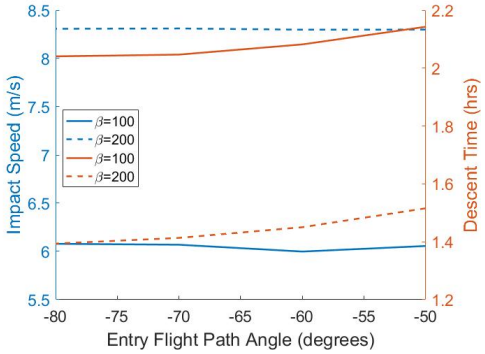

(b) Impact Speed and Descent Time vs. Entry Flight Path Angle

Figure 14: Final State Vector vs. Entry Flight Path Angle for Single Parachute, Ballistic Entry Systems

As shown in Figure 14, the entry flight path angle does play a significant factor in the landing footprint, but not as much in the impact speed or descent time. The downrange and crossrange errors also appear to be somewhat unaffected by the entry ballistic coefficient, especially for larger ballistic coefficients. This trend of decreasing variation between large ballistic coefficients appears to exist in all of the Figures in this section, indicating that a large ballistic coefficient provides some benefit to certain mission parameters such as descent time and landing error, but the benefit decreases as the ballistic coefficient is increased further and further.

3.3.2 Mid-$\frac{L}{D}$ Entry

Only one ballistic coefficient of $200 kg/m^2$ is considered in this section due to the expected similarity in the trend associated with variations in this parameter. This would likely represent a large robotic mission to Titan, such as the Titan Submarine concept [4]. In addition, the trends analyzed for entry flight path angle variations in Figure 14 are assumed to be either similar or even exacerbated by a nonzero lift-to-drag ratio and are thus not analyzed again until Double Parachute systems are considered in Section 3.4.

To begin, Figure 15 shows the final state vector for a moderate lifting body as a function of the diameter ratio. For investigations regarding moderate lift-to-drag ratios, a value of $\frac{L}{D} = 0.24$ is taken in order to match a lifting body similar to the Mars Science Laboratory (MSL) [15].

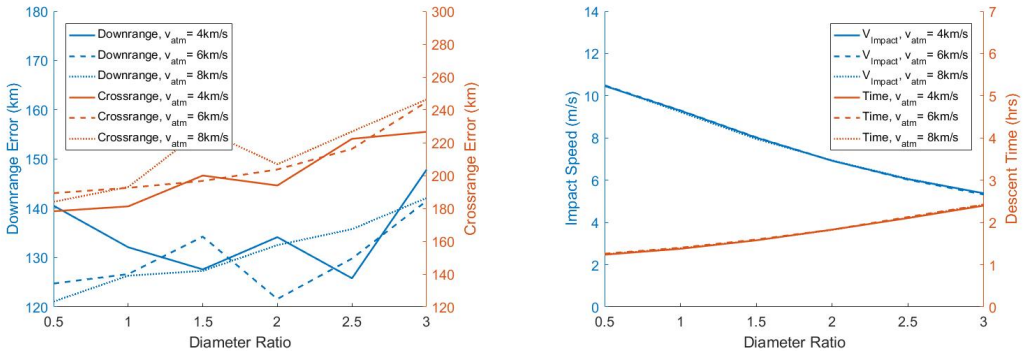

(a) Downrange and Crossrange Errors vs. Diameter Ratio

(b) Impact Speed and Descent Time vs. Diameter Ratio

Figure 15: Final State Vector vs. Diameter Ratio for Single Parachute, Moderate Lifting Body

While less definitive than in Figure 12, the trend remains the same; larger diameter ratios increase the downrange and crossrange errors as well as the descent time, while decreasing the impact speed. In addition, the length scale in the downrange and crossrange error is small enough such that it appears the entry velocity again plays a minimal role in the landing footprint.

In fact, Figure 15b indicates that the entry velocity does not influence the maximum expected impact speed or descent time at all, which, in fact, is mirrored in Figure 13 as well.

As was the case for ballistic entry, the atmospheric scale height on Titan is large enough to the point that the entry velocity plays a minimal role in the equations of motion after the initial parachute has inflated. This is because the thick atmosphere and low gravity ensure that the vehicle reaches supersonic speeds at a high altitude, at which point a parachute must be deployed for stability purposes; therefore, regardless of the entry velocity, there is sufficient distance traveled under parachute descent to dominate both the total descent time and the impact speed.

Uncertainties in the entry velocity are not discussed for moderate and high-lifting bodies with a single parachute. This is because, as discovered, the trends in the landing ellipse, impact speed, and descent time are largely similar between lifting body geometries. As such, it is expected that the entry uncertainty analysis performed in Section 3.3.1 yields sufficient data to get a rough idea of the trajectory behavior for any sort of lifting body considered for entry at Titan.

3.3.3 High-$\frac{L}{D}$ Entry

While heritage spherecone technology would be hard pressed to deliver an aeroshell with a lift-to-drag ratio above 0.5, unique entry vehicle shapes can and should be considered for robotic entry at ocean worlds to accommodate for the necessarily distinctive payloads that will be delivered to such planetary bodies. Fortunately, as discussed in Section 2.3.3, significant work has already gone into studying such shapes for aeroassist maneuvers at Earth, but this investigation seeks to define a purpose for these vehicles on missions at other solar system bodies such as Titan, Enceladus, and Europa. In this investigation, a high lifting body is assumed to have a lift-to-drag ratio of 1.17, a value cited for SO2P 4-4 concept [3]. As such, Figure 16 shows the final state vector parameters as a function of diameter ratio for high-$\frac{L}{D}$ bodies.

Figure 16a shows the same trend as previously analyzed; larger diameter ratios tend to increase the landing error for a given entry velocity. Interestingly enough, Figure 16b indicates that the entry velocity plays a non-negligible role in the descent time, unlike for ballistic and moderate lifting bodies. The impact speed is still largely unaffected except at low diameter ratios; although realistically such diameter ratios would seldom be used since the expected impact speed becomes a potential design constraint.

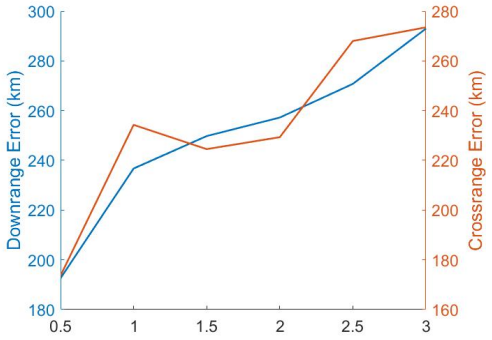

(a) Downrange and Crossrange Errors vs. Diameter Ratio at $V_{atm} = 4km/s$

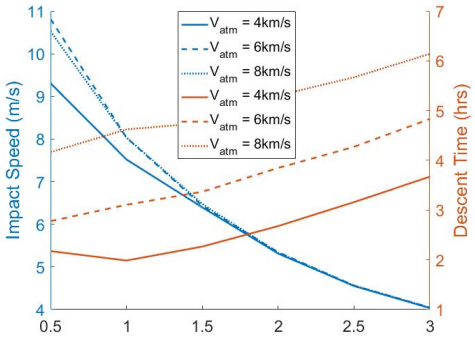

(b) Maximum Expected Impact Speed and Descent Times at $V_{atm} = 4km/s$

Figure 16: High-$\frac{L}{D}$ Vehicle Final State Vector vs. Diameter Ratio

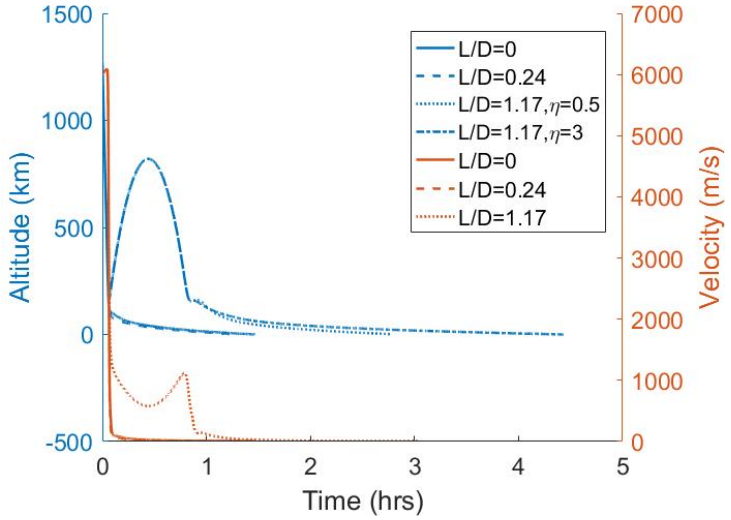

Figure 17: Altitude and Velocity vs. Descent Time for Various Lift-to-Drag Ratios

The behavior of high lifting bodies is described by Figure 17. The high lift-to-drag ratio causes a large increase in altitude before the parachute inflation mach number is reached. As the entry velocity increases, this altitude gain becomes larger and may even result in the entry vehicle skipping out of the atmosphere if the entry velocity is large enough. This causes the downrange and crossrange errors to become inconsistent and less reliable than the upward trend seen at an entry velocity of 4 km/s. Due to this inconsistency, it is suggested that more in-depth analysis is performed for these vehicles in a Titan entry environment. Due to the inconsistency presented in Section 3.3.3, the marginal benefit to heat rate parameters shown in Section 3.1, and the consistently larger landing footprints analyzed between Sections 3.3.1 and 3.3.2, it is argued that in most cases ballistic spherecone bodies are ideal for general EDL operations at Titan. This is bolstered by the argument that hypersonic guidance is relatively fruitless, as

parachute descent is shown to dominate the trajectory and final state vector. Therefore, the complex system requirements of a lifting body do not provide sufficient benefit to justify their usage for a Titan mission.

3.3.4 Entry Uncertainty Analysis

As discussed in Section 2.3.1, uncertainties in the entry state vector can likely cause large perturbations from the nominal, desired trajectory. To illustrate this point, if the 1σ uncertainty in entry altitude is only 1%, the vehicle can travel up to $12.7km$ farther or less than it was designed for. An extra $12km$ of parachute descent can increase the landing footprint by several kilometers, and a vehicle that travels $12km$ less than initially intended could cause guidance issues, premature parachute deployment, and other risky consequences.

Entry Uncertainty propagation analysis is performed by varying the value of the standard deviation for the entry state vector, mainly the uncertainties in the entry altitude, entry velocity, and entry flight path angle. The variations range from $\pm$ several percent of the Huygens entry uncertainty values. All figures depict the 1σ uncertainties on the x-axes. To begin, Figure 18 shows the final state vector parameters as functions of the entry altitude uncertainty.

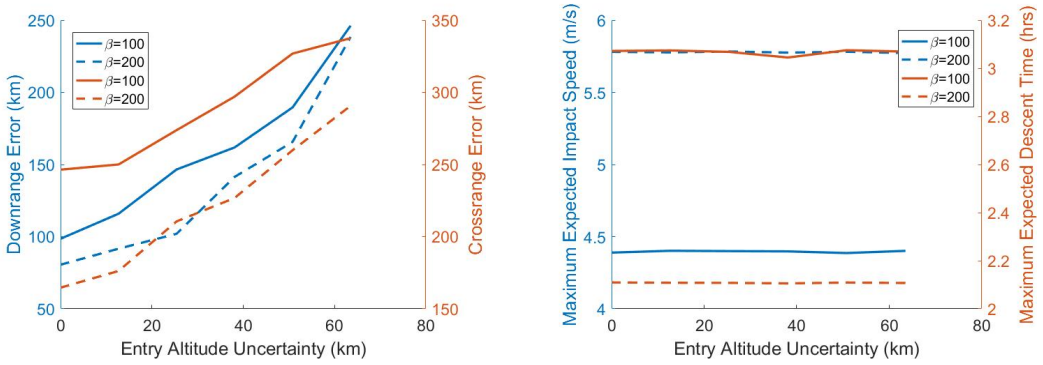

(a) Downrange and Crossrange Errors vs. Entry Altitude Uncertainty

(b) Maximum Expected Impact Velocity and Descent Times vs. Entry Altitude Uncertainty

Figure 18: Final State Vector vs. Entry Altitude Uncertainty for Single Parachute Systems

As shown in Figure 18, increasing uncertainties in the altitude of atmospheric entry significantly widens the landing footprint, the severity of which depends, as usual, on the entry ballistic coefficient.

The impact speed and descent time are negligibly affected by the entry uncertainty, which has been an expected trend for Single Parachute systems in general. Again, this is due to Titan's large scale height causing the parachute descent to dominate the trajectory.

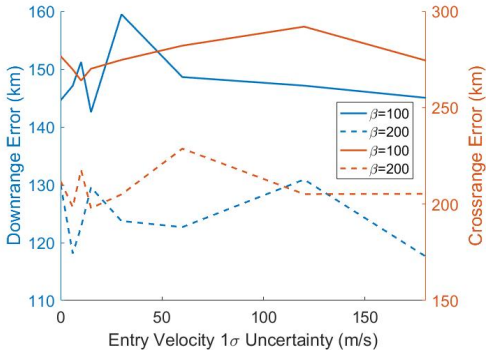

(a) Downrange and Crossrange Errors vs. Entry Velocity Uncertainty

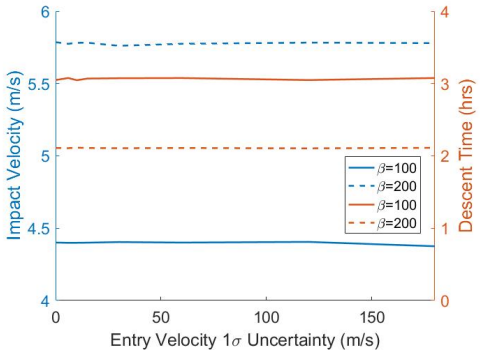

(b) Impact Velocity and Descent Times vs. Entry Velocity Uncertainty

Figure 19: Final State Vector vs. Entry Velocity Uncertainty for Single Parachute Systems

Figure 19 shows the final state vector parameters in question as functions of the entry velocity uncertainty. As usual, the maximum expected impact velocity and descent time are negligibly affected. The downrange and crossrange errors are noticeably affected; however, there is no clear trend in the data to suggest that a larger uncertainty in the entry velocity will negatively impact a vehicle's landing footprint. Of course, as discussed in Section 3.1, a larger entry velocity increases the maximum expected peak stagnation point heat rate. Therefore, while the uncertainty in the entry velocity may not affect the final state vector, it is potentially limiting from an aerothermodynamics standpoint.

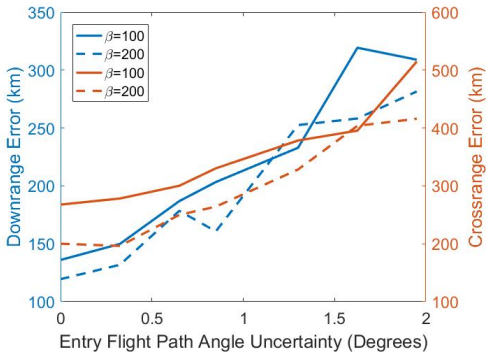

(a) Downrange and Crossrange Errors vs. Entry FPA Uncertainty

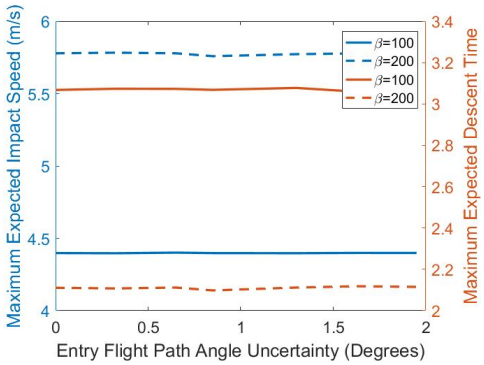

(b) Impact Velocity and Descent Times vs. Entry FPA Uncertainty

Figure 20: Final State Vector vs. Entry Flight Path Angle Uncertainty for Single Parachute Systems

Similar to Figure 18, the uncertainty in the entry flight path angle plays a negligible role in the maximum expected impact speed and descent time; however, larger entry flight path angle uncertainties are shown to increase the downrange and crossrange errors. In addition, it appears that the entry ballistic coefficient does not have as large of an impact on the landing footprint as

other variations in the entry state vector do. There is typically a noticeable difference between ballistic coefficients which is not depicted in Figure 20a.

Therefore, minimal errors in the entry altitude and entry flight path angle are desired for the most accurate landing footprints, whereas the entry velocity uncertainty has an inconclusive effect on the landing footprint. In all cases of variations in the entry state vector uncertainty, the impact speed and descent time is negligibly affected.

3.4 Two-Parachute Systems

Realistically, most EDL systems at Titan will be equipped with multiple parachutes. This is done by deploying a low diameter ratio Pilot parachute for stability in the supersonic flow regime, and then a larger, main parachute at a lower altitude and velocity. This allows for multiple diameter ratios to theoretically decrease descent time and the landing footprint without compromising impact speed. The main parachute is usually deployed at a specific mach number, velocity, or altitude, to ensure the parachute is deployed with ample time to reach the ground. This section will investigate the efficacy of multiple parachute systems and the proposed benefits.

The inflation of the second parachute can be most readily triggered by a specified velocity or altitude. For example, the Huygens Probe released it's main parachute at approximately 100 m/s [7]. This investigation analyzes the effect of varying a velocity trigger on the final state vector in addition to the diameter ratio of the main parachute. While the first parachute, referred to as the pilot parachute, could be analyzed with its own diameter ratio, a large pilot chute would result in excessive descent times and landing errors. The only realistic utilization of such a large pilot chute would be to sample the atmosphere and/or wind speeds, and this would be much better performed by an advanced conept design such as the Montgolfier Balloon, which was proposed as part of the TSSM design [14].

In order to investigate the aforementioned claims, the diameter ratio is studied as it was in Section 3.3. In addition, a velocity trigger is used to determine when to deploy the main parachute and is thus varied to analyze the effects on the final state vector. For all scenarios not analyzing the velocity trigger it is set to $40 m/s$, as this was the velocity trigger for the final parachute on the Huygens Probe [7]. Therefore, only variations in the main parachute are considered. For all simulations, the pilot chute diameter is assumed to be equal to the reference diameter of the aeroshell to prevent a large increase in drag area. To begin, Figure 21 shows the landing footprint as a function of diameter ratio for a ballistic entry vehicle.

3.4.1 Ballistic Entry

The effect of varying the main parachute diameter ratio is first considered in Figures 21a-21d.

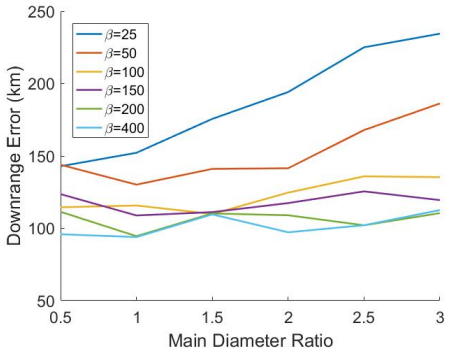

(a) Downrange Error vs. Diameter Ratio for $V_{atm} = 4km/s$

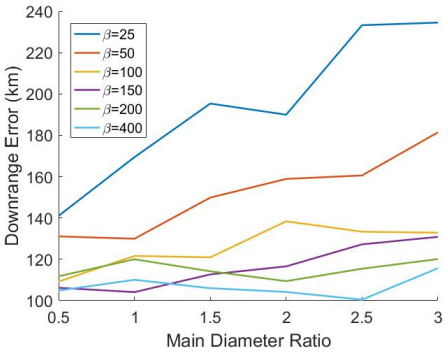

(b) Downrange Error vs. Diameter Ratio for $V_{atm} = 8km/s$

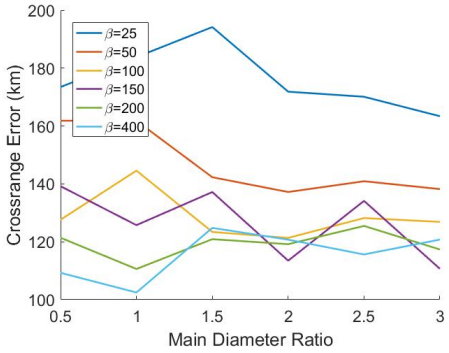

(c) Crossrange Error vs. Diameter Ratio for $V_{atm} = 4km/s$

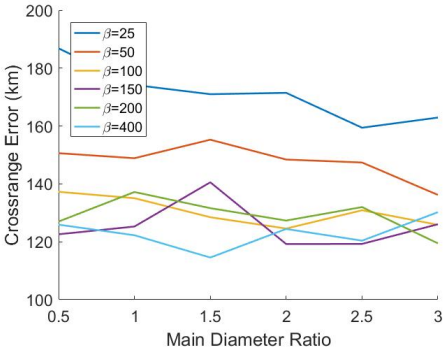

(d) Crossrange Error vs. Diameter Ratio for $V_{atm} = 8km/s$

Figure 21: Downrange and Crossrange Errors vs. Diameter Ratios for Two Parachute Systems and Ballistic Entry

While Figures 21a and 21b demonstrate that the downrange error for smaller ballistic coefficients tends to increase for larger main parachute diameter ratios, Figures 21c and 21d show inconsistency in the crossrange error as a function of diameter ratio and ballistic coefficient. This may be an artifact of the wind speeds at low altitudes and the specific entry azimuth angle of the vehicle; regardless, mission concepts in the future should be mindful of these inconsistencies. Finally, there appears to be little variation in the downrange and even crossrange error across different entry velocities, as anticipated based on the results in Section 3.3.

Figure 22 depicts the maximum expected impact speed and descent time as a function of main parachute diameter ratio for two different entry velocities. Just as in Section 3.3.1, the impact velocity and total descent time are largely unaffected by the entry velocity due to the large scale height and low gravity on Titan.

While the same trends are shown for two-parachutes systems as for single parachute systems,

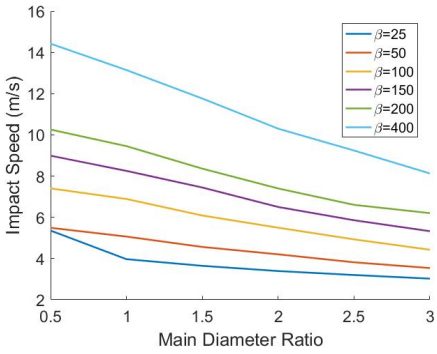

(a) Impact Speed vs. Diameter Ratio for $V_{atm} = 4km/s$

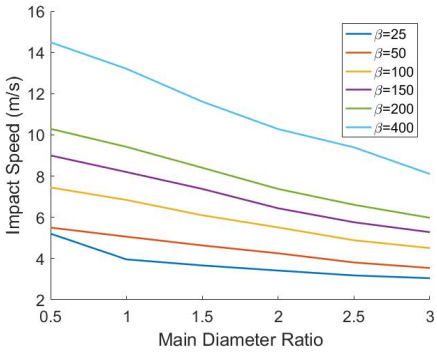

(b) Impact Speed vs. Diameter Ratio for $V_{atm} = 8km/s$

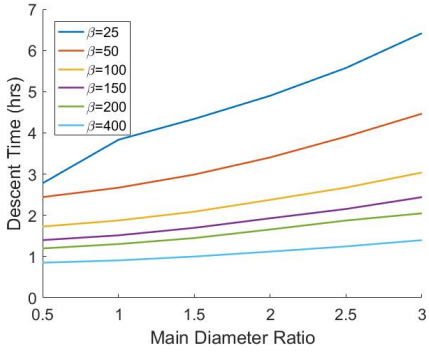

(c) Descent Time vs. Diameter Ratio for $V_{atm} = 4km/s$

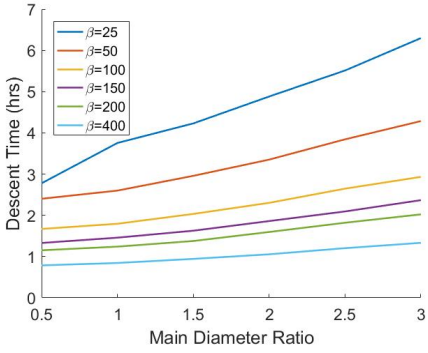

(d) Descent Time vs. Diameter Ratio for $V_{atm} = 8km/s$

Figure 22: Maximum Expected Impact Speed and Descent Time vs. Diameter Ratios for Two Parachute Systems and Ballistic Entry

the final state vectors must be compared directly to determine any benefits of two-parachute systems. Therefore, Figure 23 shows the final state vector for two different ballistic coefficients against single and two-parachute systems.

Figures 23c and 23d show that the impact speed and descent times are negligibly affected by the addition of another parachute. However, Figures 23a and 23b show that there is a noticeable benefit to the landing footprint for two-parachute systems for almost every diameter ratio. Therefore, while they are more complex, systems with multiple, staged, parachutes tend to have a smaller landing footprint than single parachute systems.

In order to understand the influence of the velocity trigger on the final state vector, Figure 24 plots the final state vector parameters against the Velocity Trigger velocity as functions of both diameter ratio and ballistic coefficient.

Figure 24 demonstrates that the velocity trigger plays a noticeable, if not inconsistent role, on the final state vector. The downrange error is affected more by the diameter ratio across various velocity triggers than the crossrange error is, which reflects the results shown in Figure

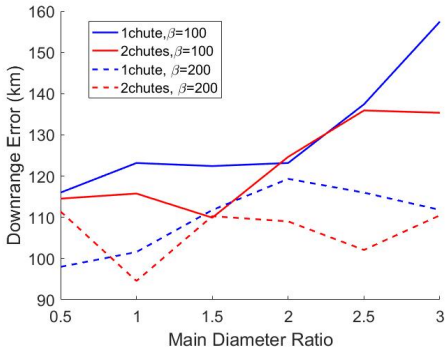

(a) Comparison of Downrange Footprint

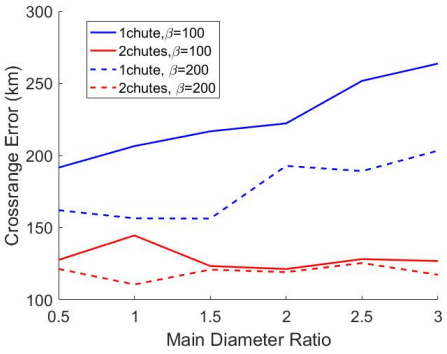

(b) Comparison of Crossrange Footprint

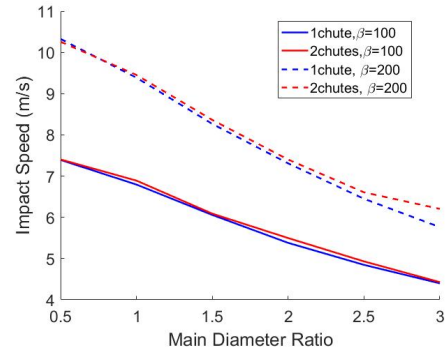

(c) Comparison of Impact Speed

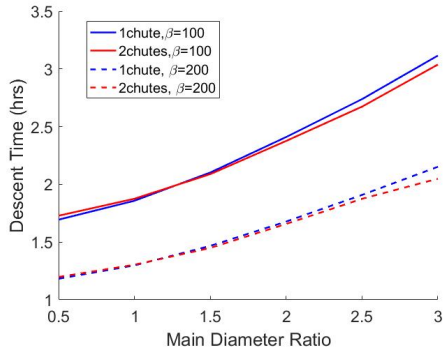

(d) Comparison of Descent Time

Figure 23: Comparison of Number of Parachutes for Ballistic Entry Final State Vector vs. Parachute Diameter Ratio

21. In addition, the downrange and crossrange errors tend to be increased for a larger parachute inflation velocity trigger with some inconsistencies in the trends. Similar behavior is observed for the landing footprint as a function of various ballistic coefficients. It appears, however, that the crossrange error is more dependent on the ballistic coefficient than the diameter ratio. The data suggest that an optimal velocity trigger speed is between $60m/s$ and $80m/s$, but this should be analyzed further for any mission planning.

Figures 24b and 24d show the maximum expected impact speed and descent time plotted against the velocity trigger. It appears that the impact speed is affected by the velocity trigger more so than the descent time for various diameter ratios. However, this trend is most noticeable for low diameter ratios, yielding an impact speed that may put troubling constraints on the vehicle design. In all other cases, the impact speed and descent time are barely influenced by the velocity trigger.

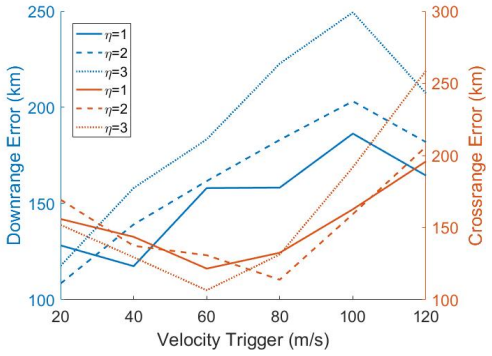

(a) Downrange and Crossrange Errors vs. Velocity Trigger for Various Diameter Ratios

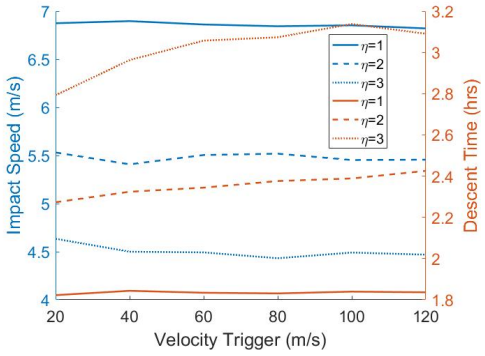

(b) Impact Speed and Descent Time vs. Velocity Trigger for Various Diameter Ratios

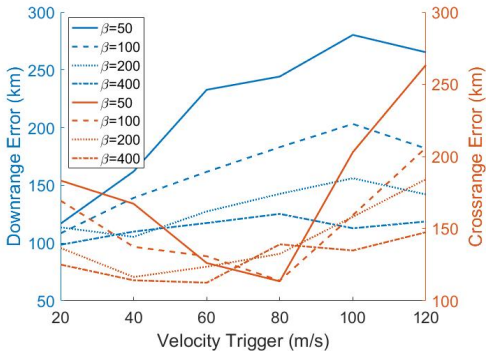

(c) Downrange and Crossrange Errors vs. Velocity Trigger for Various β

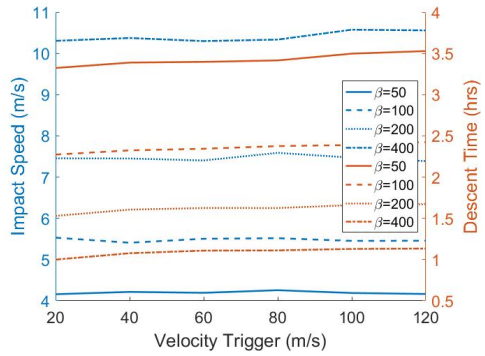

(d) Impact Velocity and Descent Time vs. Velocity Trigger for Various β

Figure 24: Final State Vector Parameters vs. Velocity Trigger as functions of Diameter Ratio and Ballistic Coefficient for Ballistic Entry

3.4.2 Mid-$\frac{L}{D}$ Entry

In a similar approach to Section 3.4.1, the effect of varying the diameter ratio on the final state vector for various ballistic coefficients is first considered for moderate lifting bodies in Figure 25.

Similar to Figure 21, the downrange error tends to increase with main parachute diameter ratio for smaller ballistic coefficients, while the crossrange error data is inconclusive. While the entry velocity typically has played a negligible role in the final state vector results, Figure 25 shows that the entry velocity disrupts this trend in the data; a larger entry velocity appears to increase the downrange and crossrange errors for moderate lifting bodies noticeably for each diameter ratio. This may be a result of the fact that the lift force keeps the entry vehicle at a higher altitude, while the pilot parachute is fixed to be the same size as the aeroshell diameter, causing the vehicle to deploy its parachutes at higher altitudes and thus increase the landing footprint. In order to see if this effect is portrayed in the impact speed and descent times, Figure 26 displays the maximum expected impact speed and descent time as a function of the

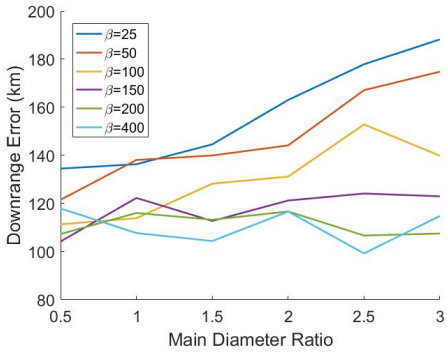

(a) Downrange Error vs. Diameter Ratio for $V_{atm} = 4m/s$

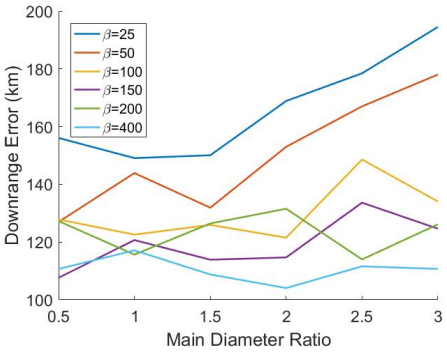

(b) Downrange Error vs. Diameter Ratio for $V_{atm} = 8km/s$

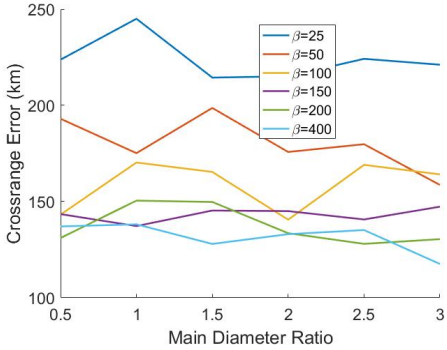

(c) Crossrange Error vs. Diameter Ratio for $V_{atm} = 4km/s$

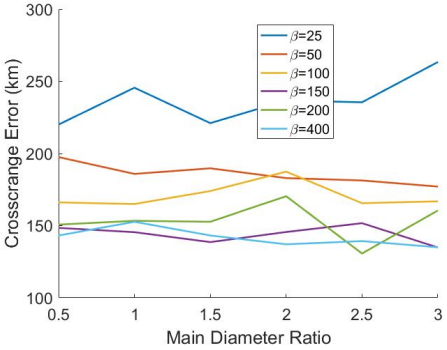

(d) Crossrange Error vs. Diameter Ratio for $V_{atm} = 8km/s$

Figure 25: Downrange and Crossrange Errors vs. Diameter Ratio for Moderate Lift, Two Parachute Systems

main parachute diameter ratio.

Figure 26 contradicts the previous theory; the impact speed and descent time are negligibly affected by the entry velocity as usual. The same trends in the impact speed and descent time that were analyzed for ballistic entry vehicles are reflected in Figure 26, as well. Next, the comparison between the number of parachutes for an EDL system is depicted in Figure 27.

Figure 27 shows again that the added parachute decreases the landing footprint noticeably compared to single parachute systems for every diameter ratio. In addition, the impact speed and descent time are barely affected by the added parachute.

The data in Figure 28 demonstrates that the velocity trigger has a somewhat more consistent effect on the landing footprint than it did for ballistic entry vehicles. The downrange error is significantly more consistent, and clearly increases for larger velocity triggers across various ballistic coefficients, whereas the crossrange error does increase at large velocity triggers, but in inconsistent at lower deployment speeds. The downrange error is slightly inconsistent at low velocity triggers for various diameter ratios, but still appears to have an increasing trend as a

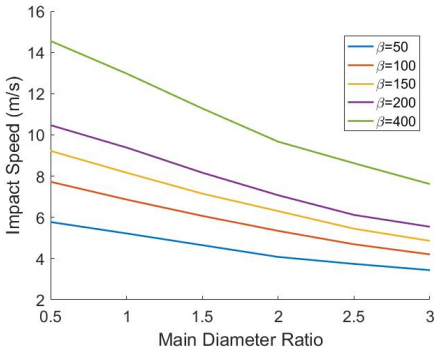

(a) Impact Speed vs. Diameter Ratio for $V_{atm} = 4m/s$

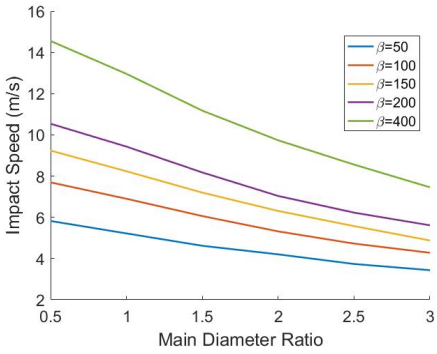

(b) Impact Speed vs. Diameter Ratio for $V_{atm} = 8km/s$

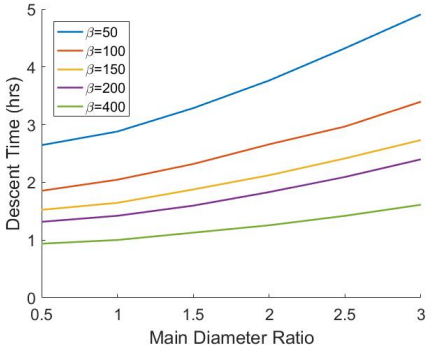

(c) Descent Time vs. Diameter Ratio for $V_{atm} = 4km/s$

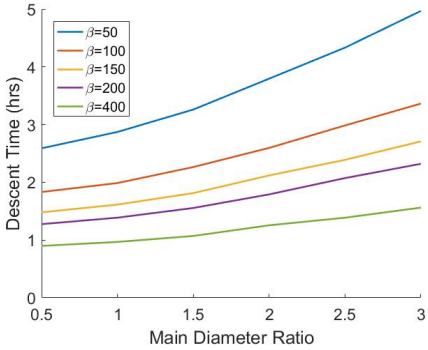

(d) Descent Time vs. Diameter Ratio for $V_{atm} = 8km/s$

Figure 26: Impact Speed and Descent Time vs. Diameter Ratio for Moderate Lift, Two Parachute Systems

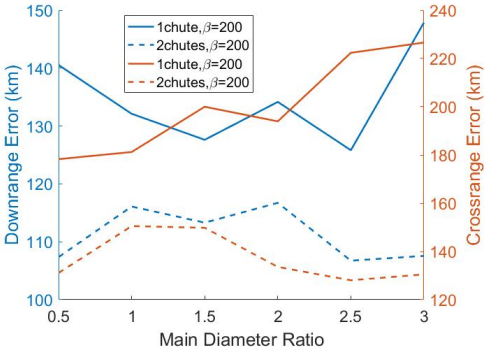

(a) Comparison of Downrange and Crossrange Error

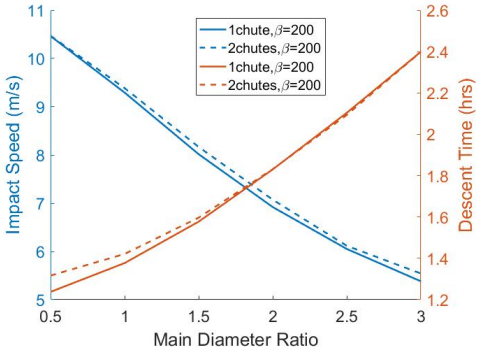

(b) Comparison of Impact Speed and Descent Time

Figure 27: Comparison of Number of Parachutes for Moderate Lifting Body Final State Vector vs. Parachute Diameter Ratio

function of the parachute deployment velocity. The crossrange error for various diameter ratios is still inconsistent, potentially even more so than for various ballistic coefficients.

Additionally, the velocity trigger appears to have a noticeable effect on the descent time but not as much on the impact velocity across various ballistic coefficients. Meanwhile, the diameter

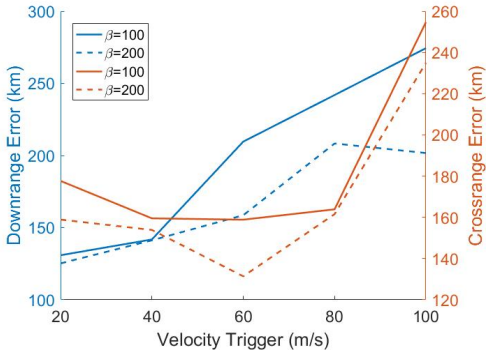

(a) Downrange and Crossrange Errors vs. Velocity Trigger

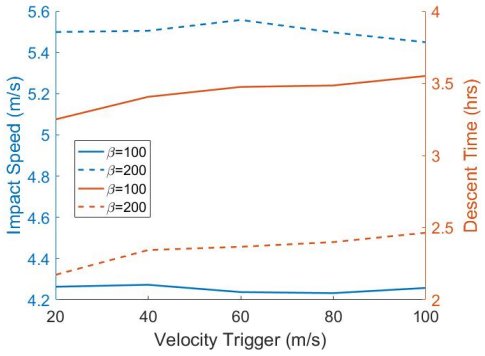

(b) Impact Speed and Descent Time vs. Velocity Trigger

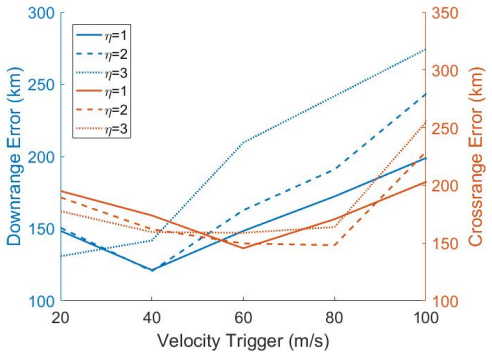

(c) Downrange and Crossrange Errors vs. Velocity Trigger

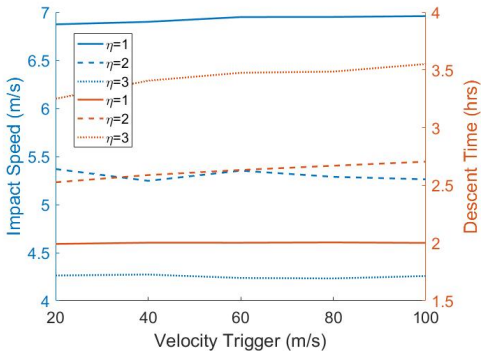

(d) Impact Speed and Descent Time vs. Velocity Trigger

Figure 28: Final State Vector vs. Velocity Trigger for Moderate Lift, Two Parachute Systems

ratio does not seem to play a significant role in the impact speed or the descent time.

Finally, High lift-to-drag ratio bodies will be considered in Section 3.4.3 to confirm whether or not the analyzed trends remain the same.

3.4.3 High-$\frac{L}{D}$ Entry

As shown in Section 3.3.3, the large lift-to-drag ratio has an anomalous effect on the landing footprint as a function of diameter ratio due to the large increase in altitude and velocity just before parachute inflation. It is theorized that this phenomenon will be the same for two-parachute systems, although potentially not as severe due to the presence of the Pilot parachute. To begin analyzing this theory, Figure 29 plots the final state vector parameters against the diameter ratio.

The data shown in Figure 29a is very inconsistent; it shows a slight increasing trend in the downrange and crossrange error at a ballistic coefficient of $100\frac{kg}{m^2}$, but at a higher ballistic coefficient there is no discernible detriment to having a larger diameter ratio. This is counter intuitive and should be studied further when designing for a high lifting body mission. Ad-

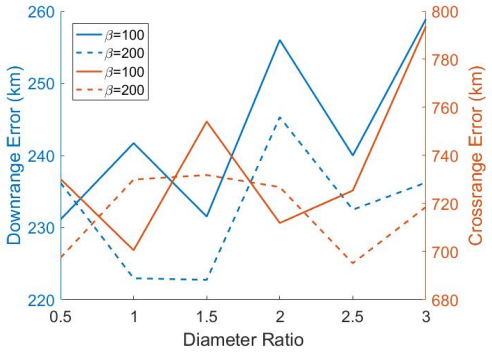

(a) Downrange and Crossrange Error vs. Diameter Ratio for $V_{atm} = 6m/s$

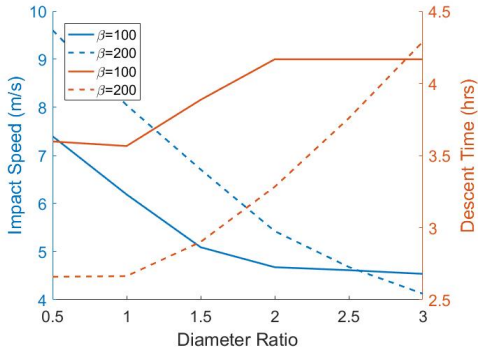

(b) Impact Speed and Descent Time vs. Diameter Ratio for $V_{atm} = 6km/s$

Figure 29: Final State Vector vs. Diameter Ratio for High Lift, Two Parachute Systems

ditionally, the impact speed and descent times appear to show clear trends that reflect those from previous sections. It appears, however, that at low ballistic coefficients the two parameters plateau at higher diameter ratios. Given the counter intuitive data from Figure 29b, this too should be considered in any mission and vehicle design. In order to see how the parachute systems influence the final state vector for high lifting bodies, Figure 30 plots the final state vector parameters against diameter ratio for single and two-parachute systems.

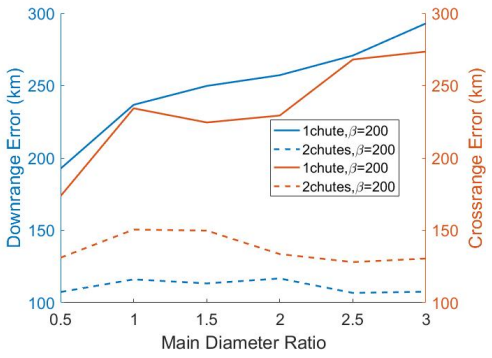

(a) Comparison of Landing Footprint

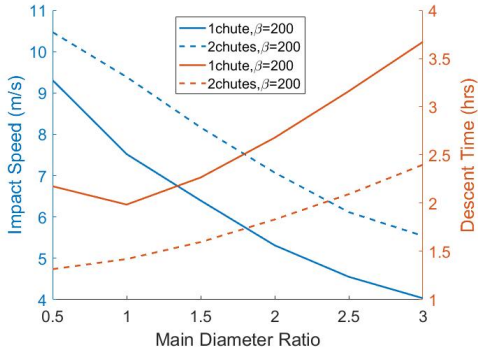

(b) Comparison of Impact Speed and Descent Time

Figure 30: Comparison of Number of Parachutes for High Lifting Body Final State Vector vs. Parachute Diameter Ratio

Again, it appears that the addition of a second parachute decreases the landing footprint and descent time compared to single parachute systems. Oddly enough, the second parachute appears to increase the impact speed for all diameter ratios. This discrepancy may be a result of small diameter ratio pilot chute being unable to decelerate the entry vehicle as well as a single, larger parachute. Regardless, it should be analyzed further when designing a high lifting vehicle, especially when the increased impact speed may further constrain the vehicle and mission design.

In order to assess the effect of the main parachute inflation velocity trigger, Figure 31 plots the final state vector parameters against the main parachute inflation velocity trigger.

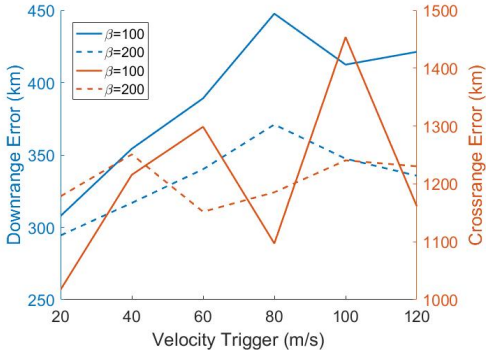

(a) Downrange and Crossrange Errors vs. Velocity Trigger

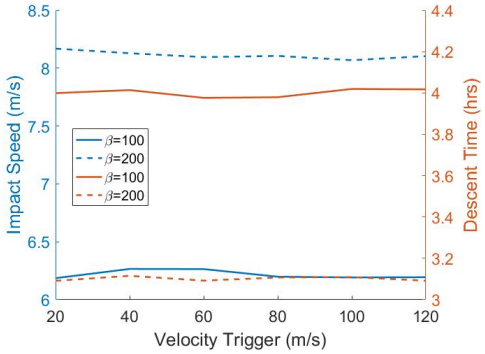

(b) Impact Speed and Descent Time vs. Velocity Trigger

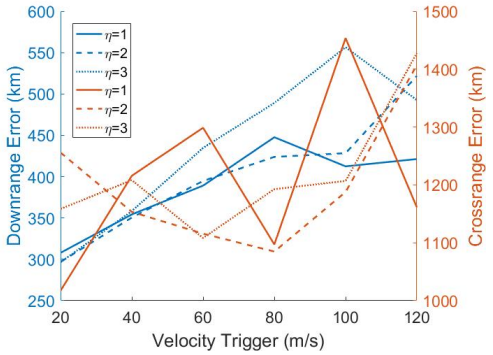

(c) Downrange and Crossrange Errors vs. Velocity Trigger

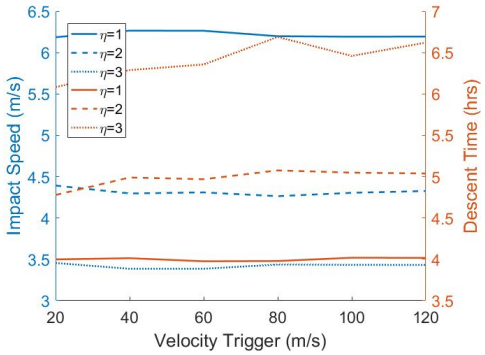

(d) Impact Speed and Descent Time vs. Velocity Trigger

Figure 31: Final State Vector vs. Velocity Trigger for High Lift Systems and Various Ballistic Coefficients and Diameter Ratios

In general, there is a positive correlation between the landing footprint and velocity trigger; however, the crossrange error data at $100\frac{kg}{m^2}$ is wildly erratic, while the crossrange data at $200\frac{kg}{m^2}$ is also variable, especially across various diameter ratios. This unpredictability in the crossrange error was also noticed in Section 3.4.2, and is likely just an artifact of the entry azimuth. Of course, it should be analyzed further for mission designs, as usual. The downrange error is slightly inconsistent, but still tends to increase with larger velocity triggers.

The impact speeds and descent times are only slightly affected by the velocity trigger at low diameter ratios, while for all other scenarios they are negligibly affected by the velocity trigger, as noted in both Section 3.4.1 and Section 3.4.2. These trends are truly indicative of how the dense atmosphere and low gravity combine to create such a unique entry environment on Titan. The impact velocity is barely affected when the main parachute is opened at only $20m/s$, compared to being opened at $120m/s$, even with a pilot parachute with a diameter ratio

of 1. There may be noticeable changes to the impact speed and descent time as a function of the velocity trigger were the pilot chute diameter ratio to be lowered below 1; however, there may be stability issues arising in the supersonic regime requiring further testing.

Now that a range of lift-to-drag ratios have been analyzed, the uncertainty in the entry state vector will be analyzed in Section 3.4.4 as it was in Section 3.3.4.

3.4.4 Entry Uncertainty Analysis

Uncertainties in the entry state vector were shown to have significant effects on the final state vector in Section 3.3.4; this section seeks to understand if these same uncertainties cause similar or different changes to the final state vector for two parachute systems as opposed to single parachute systems. It was previously observed that, for all lift-capable entry vehicles, the additional parachute decreased the landing footprint, but had relatively no effect on the impact speed or descent time, except for high lifting bodies. It is assumed these same trends will carry over to uncertainties in the entry state vector as they did in Section 3.3.4. Therefore, there won't be a comparison with single parachute systems for the entry uncertainty analysis. Figure 32 shows the final state vector as a function of entry altitude uncertainty.

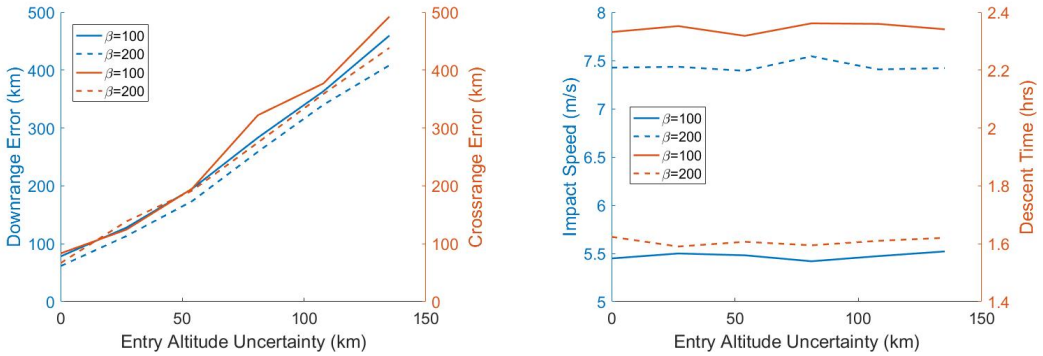

(a) Downrange and Crossrange Errors vs. Entry Altitude Uncertainty

(b) Impact Speed and Descent Time vs. Entry Altitude Uncertainty

Figure 32: Final State Vector vs. Entry Altitude Uncertainty for Ballistic, Two Parachute Systems

It is clear that the entry altitude uncertainty plays a noticeable role in the downrange and crossrange errors, and a negligible role in the impact speed and descent time. It also appears that the entry ballistic coefficient does not significantly impact the landing footprint error for all tested entry altitude uncertainties. This is due to the large scale height on Titan; the vehicle trajectory is dominated by parachute descent and therefore the uncertainty in the altitude of atmospheric entry plays a minimal role between ballistic coefficients. It also appears from Figure

32b that the entry altitude uncertainty plays a minimal role in the impact speed and descent time, as usual.

Next, the uncertainty in the entry velocity will be analyzed in Figure 33.

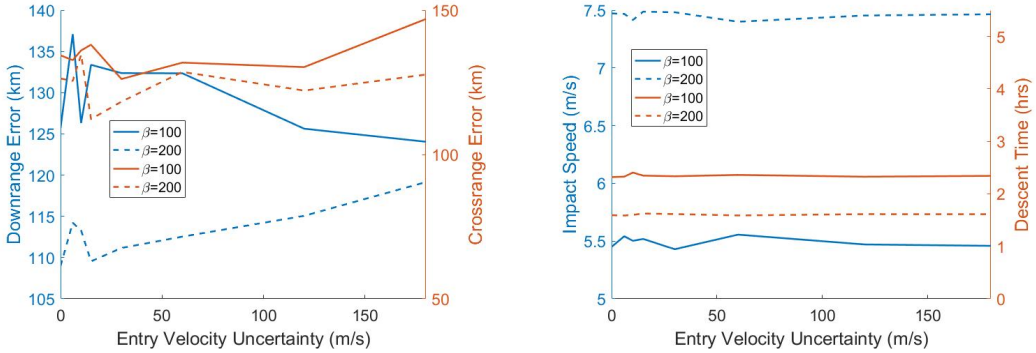

(a) Downrange and Crossrange Errors vs. Entry Velocity Uncertainty

(b) Impact Speed and Descent Time vs. Entry Velocity Uncertainty

Figure 33: Final State Vector vs. Entry Velocity Uncertainty for Ballistic, Two Parachute Systems

Figure 33a shows that the downrange and crossrange errors are inconsistently affected by the entry velocity uncertainty. While a ballistic coefficient of $100\frac{kg}{m^2}$ causes the downrange error to increase with entry velocity uncertainty, a ballistic coefficient of $200\frac{kg}{m^2}$ is shown to decrease the downrange error as a function of increasing entry velocity uncertainty. In addition, Section 3.3.4 showed that the entry velocity uncertainty did not play a definitive role in the landing footprint. However, it has been a noticeable trend that, in general, the entry velocity plays a negligible role in the final state vector. Therefore, it is advised that this be studied further during mission concept designs; however, in a general sense it should be noted that the entry velocity tends not to play as big of a role in the vehicle's final state vector as other parameters such as altitude uncertainty, ballistic coefficient, and parachute diameter ratio.

The final entry uncertainty parameter that will be analyzed is the entry flight path angle. Figure 34 shows the final state vector parameters as a function of the entry flight path angle uncertainty.

Similar to how the entry altitude uncertainty did not affect the landing footprint between ballistic coefficients, the same is shown in Figure 34; larger entry flight path angle uncertainty cause an increase in both the downrange and crossrange errors while being relatively unaffected by various ballistic coefficients. Additionally, the entry flight path angle uncertainty plays a negligible role in the impact speed or descent time, as expected based on previous results concerning the impact speed and descent time.

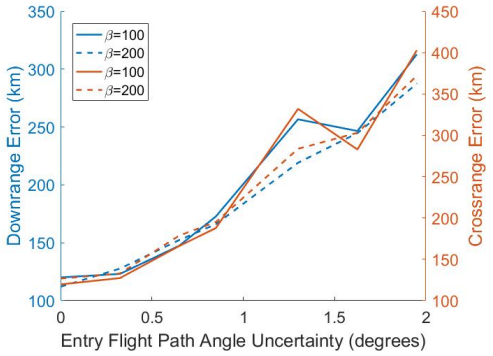

(a) Downrange and Crossrange Errors vs. Entry Flight Path Angle Uncertainty

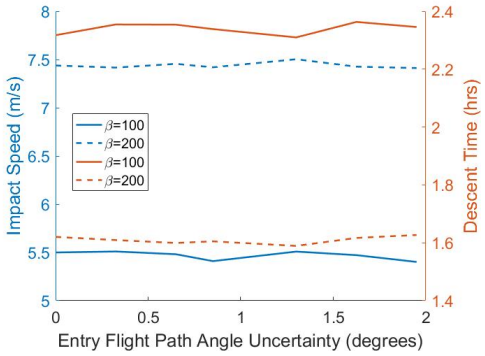

(b) Impact Speed and Descent Time vs. Entry Flight Path Angle Uncertainty

Figure 34: Final State Vector vs. Entry Flight Path Angle Uncertainty for Ballistic, Two Parachute Systems

4 Conclusions

4.1 Summary of Results

The entry velocity plays the largest role in the peak deceleration, while both the entry velocity and vehicle bluntness ratio cause the biggest impact on the maximum expected peak stagnation point heat rate and total integrated heat load. The ballistic coefficient also plays a noticeable role; however, the bluntness ratio is typically a much more flexible design constraint. In addition, shallower entry flight path angles decrease the peak heat rate, especially at higher ballistic coefficients.

It was found that, while they are more complex systems, entry vehicles equipped with two parachutes tend to have smaller landing footprints, impact speeds, and descent times than those with only a single parachute. In general, larger ballistic coefficients decreased the landing footprints and descent times while increasing impact speeds, although adding a lift capability sometimes caused these trends to vary. In addition, larger parachute diameter ratios increased the landing footprint and descent times, but decreased the impact speed.

In general, uncertainties in the entry altitude and flight path angle cause a noticeable change in the landing footprint, but a negligible change in the impact speed or descent time, while uncertainties in the entry velocity cause a variable change in the landing footprint. Although, in general, it was noted that the entry velocity plays a minimal role in the final state vector. While the uncertanties in the entry state vectors for both single and two-parachute systems were not compared, it can be assumed by analyzing the trends in Sections 3.3 and 3.4 that the two-parachute systems would cause a decrease in all parameters of the final state vector for various entry vector uncertainties.

Therefore, based on the results obtained in this investigation, an ideal entry vehicle at Titan would consist of a ballistic spherecone body entering from orbit to decrease the entry velocity and thus the peak heat and peak deceleration. Ballistic spherecone bodies are shown to be ideal because they provide the smallest landing footprint, while lifting bodies generate negligible aerothermodynamic benefits in addition to complicating the entry vehicle design.

The ideal entry vehicle would have a flight path angle similar to the Huygens Probe so as to prevent the peak heat rate or integrated heat load from becoming too large, in addition to keeping the peak deceleration to a manageable level. In addition, it would have as large of a ballistic coefficient as possible without compromising the TPS systems or aeroshell/payload

structure in order to decrease the landing footprint and descent times as much as possible.

The ideal Titan entry vehicle would be equipped with two parachutes; one pilot chute with a diameter ratio less than or equal to one, and a main parachute with a diameter ratio of at least 2. The two parachute systems would further decrease the landing footprint, while negligibly affecting the descent time and impact speed. These systems together would ideally satisfy all of the necessary constraints while landing as large of a payload to Titan as possible.

4.2 Future Work

While this investigation sought to trivialize EDL on Titan, there is still a considerable amount of work involved in planning such a mission, specifically with guidance options and vehicle aerodynamics. This thesis did not attempt to cover guidance options, although it briefly explained the benefits and flaws associated with those systems. In addition, the aerodynamic and reference geometry values were taken from literature instead of determined either analytically or computationally for verification.

It was explained in Section 1.3 that deceleration and guidance options are quite limited on Titan. However, one technology that may not be hindered by Titan's unique atmospheric and gravitational phenomena is a steerable parafoil; these parafoils would enable the vehicle to prevent severe wind drift through the application of a side force. One potential drawback is that parafoils would cause the vehicle to glide through the atmosphere, potentially generating massive downrange capabilities and footprints.

The vehicle aerodynamics were taken from the literature in order to allow for enough computational power and time to run several hundred Monte Carlo analyses in Matlab. Ideally, each vehicle geometry, especially the high-lifting bodies, would have aerodynamic databases as a function of mach number to both verify the literature, as well as produce more accurate results with mach number-dependent aerodynamic coefficients.

Finally, there are gaps in the results such as comparisons in the entry state vector uncertainties between single and two-parachute systems, and variations in ballistic coefficients, diameter ratios, aerothermodynamics, and entry velocities for the lifting body cases. Most of these results would depict the same trends shown in the ballistic entry sections; although others might provide more in-depth analysis to the unpredictable results. This investigation was meant to provide a framework for understanding the EDL tradespace on Titan, and as such all results should be verified by any mission planners seeking to gain a deeper understanding of the flight

mechanics of a specific entry vehicle concept.

References

[1] J R Cruz, R E Mineck, D F Keller, and M V Bobskill. AIAA 2003-2129 Wind Tunnel Testing of Various Disk-Gap-Band Parachutes 17 th Aerodynamic Decelerator Systems Technology Conference and Seminar 19-22 May 2003 Monterey , California. (May), 2003.

[2] A.D Fortes. Exobiological Implications of a Possible Ammonia–Water Ocean inside Titan. *Icarus*, 146(2):444–452, 2000.

[3] General Electric. Generic Aerocapture Atmospheric Entry Study. 1980.

[4] J. W. Hartwig, A. Colozza, R. D. Lorenz, S. Oleson, G. Landis, P. Schmitz, M. Paul, and J. Walsh. Exploring the depths of Kraken Mare - Power, thermal analysis, and ballast control for the Saturn Titan submarine. *Cryogenics*, 74:31–46, 2016.

[5] Ralf Jaumann, Randolph L. Kirk, Ralph D. Lorenz, Rosaly M C Lopes, Ellen Stofan, Elizabeth P. Turtle, Horst Uwe Keller, Charles A. Wood, Christophe Sotin, Laurence A. Soderblom, and Martin G. Tomasko. Geology and surface processes on titan. *Titan from Cassini-Huygens*, pages 75–140, 2010.

[6] C G Justus and Aleta Duvall. Aiaa 2003-4803 Engineering-Level Model Atmospheres for Titan and Neptune. *Aiaa*, (July):1–6, 2003.

[7] Bobby Kazeminejad, David H Atkinson, and Miguel Pe. Huygens ' entry and descent through Titan ' s atmosphere — Methodology and results of the trajectory reconstruction. 55:1845–1876, 2007.

[8] Jean-Pierre Lebreton, Olivier Witasse, Claudio Sollazzo, Thierry Blancquaert, Patrice Couzin, Anne-Marie Schipper, Jeremy B Jones, Dennis L Matson, Leonid I Gurvits, David H Atkinson, Bobby Kazeminejad, and Miguel Pérez-Ayúcar. An overview of the descent and landing of the Huygens probe on Titan. *Nature*, 438(7069):758–764, 2005.

[9] Ralph D Lorenz and Jennifer L Mann. Seakeeping on Ligeia Mare : Dynamic Response of a Floating Capsule to Waves on the Hydrocarbon Seas of Saturn ' s Moon Titan. 33(2):82–94, 2015.

[10] Ralph D. Lorenz and Claire E. Newman. Twilight on Ligeia: Implications of communications geometry and seasonal winds for exploring Titan's seas 2020-2040. *Advances in Space Research*, 56(1):190–204, 2015.

[11] Ralph D. Lorenz, Claire E. Newman, Tetsuya Tokano, Jonathan L. Mitchell, Benjamin Charnay, Sebastien Lebonnois, and Richard K. Achterberg. Formulation of a wind specification for Titan late polar summer exploration. *Planetary and Space Science*, 70(1):73–83, sep 2012.

[12] MSFC. Orbital Transfer Systems with Emphasis on Shuttle Applications 1986-1991. 73354, 1991.

[13] Giuseppe Pezzella, Giuliano Marino, and Giuseppe C. Rufolo. Aerodynamic Database Development of the ESA Intermediate Experimental Vehicle. *Acta Astronautica*, 94(1):57–72, 2014.

[14] Kim Reh, Christian Erd, Dennis Matson, Athena Coustenis, Jonathan Lunine, and Jean-Pierre Lebreton. Titan Saturn System Mission. 1:1689–1699, 2015.

[15] Mark Schoenenberger, John Van Norman, Chris Karlgaard, Prasad Kutty, and David Way. Mars Science Laboratory Entry Vehicle. *Journal of Spacecraft and Rockets*, 51(4):1076–1093, 2014.

[16] E Stofan and R Lorenz. TiME - The Titan Mare Explorer. *Aerospace ...*, pages 1–14, 2013.

[17] K. Sutton and R. a. Graves. A general stagnation-point convective heating equation for arbitrary gas mixtures. (NASA TR R-376), 1971.

[18] United Launch Alliance. *Atlas V Launch Services User's Guide*. Number March. 2010.

[19] John White. Feasibility and Tradeoff Study of an Aeromaneuvering Orbit-to-Orbit Shuttle (AMOOS). 1974.